



1 Marine Carbohydrates and Other Sea Spray Aerosol Constituents Across 2 Altitudes in the Lower Troposphere of Ny-Ålesund, Svalbard

3 Sebastian Zeppenfeld^{1*}, Jonas Schaefer², Christian Pilz², Kerstin Ebell³, Moritz Zeising⁴, Frank
 4 Stratmann², Holger Siebert², Birgit Wehner², Matthias Wietz^{4,5,6}, Astrid Bracher^{4,7}, and
 5 Manuela van Pinxteren¹

6 1 Atmospheric Chemistry Department (ACD), Leibniz Institute for Tropospheric Research (TROPOS),
 7 Leipzig, Germany

8 2 Atmospheric Microphysics (AMP), Leibniz Institute for Tropospheric Research (TROPOS), Leipzig,
 9 Germany

10 3 Institute for Geophysics and Meteorology, University of Cologne, Cologne, Germany

11 4 Alfred Wegener Institute Helmholtz Centre for Polar and Marine Research, Bremerhaven, Germany

12 5 Max Planck Institute for Marine Microbiology, Bremen, Germany

13 6 Institute for Chemistry and Biology of the Marine Environment, University of Oldenburg, Oldenburg,
 14 Germany

15 7 Institute of Environmental Physics, University of Bremen, Bremen, Germany

16

17 *Correspondence to: Sebastian Zeppenfeld (zeppenfeld@tropos.de)

18

19

20

21 Abstract

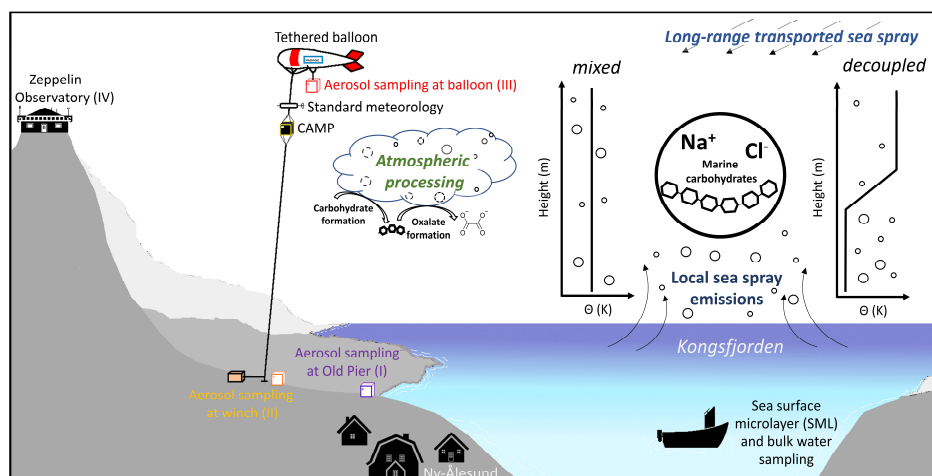
22 Marine combined carbohydrates in aerosol particles (CCHO_{aer}) have the potential to influence
 23 cloud formation and properties, but it remains unclear to what extent they reach altitudes
 24 relevant for cloud processes. Balloon-borne measurements of major sea spray aerosol (SSA)
 25 constituents, including sodium (Na⁺_{aer}) and CCHO_{aer}, were conducted in autumn 2021 and
 26 spring 2022 in Ny-Ålesund (Svalbard). Total suspended particles were collected at 321–1112 m,
 27 covering both the marine boundary layer and the free troposphere, with Na⁺_{aer} ranging 23–
 28 850 ng m⁻³ and CCHO_{aer} 3.8–274 ng m⁻³. The chemical composition of balloon-borne aerosol
 29 samples was compared with synchronized ground level measurements at the balloon's winch
 30 (Na⁺_{aer}: 35–3710 ng m⁻³; CCHO_{aer}: 1.9–194 ng m⁻³), and at the Old Pier (Na⁺_{aer}: 140–1470 ng m⁻³;
 31 CCHO_{aer}: 1.6–10.0 ng m⁻³), where freshly emitted SSA particles were sampled. Surface
 32 seawater from the Kongsfjorden was analyzed to evaluate the sea-air transfer of marine
 33 CCHO. Air mass histories, atmospheric mixing, and cloud conditions were evaluated for three
 34 selected cases to explain vertical concentration patterns. A strong correlation (R=0.78,



35 $p < 0.001$) between combined xylose ($< 0.2\text{--}14.1\text{ ng m}^{-3}$) in CCHO_{aer} and oxalate_{aer} ($< 1\text{--}67\text{ ng m}^{-3}$)
 36 across all altitudes, suggests either coproduction or a connection through atmospheric
 37 processing. These results provide a first comprehensive picture of local primary sea-air
 38 transfer of marine combined carbohydrates and highlight the roles of long-range transport,
 39 in-situ formation, and chemical aging in shaping their atmospheric distribution.

40

41



42



43 1. Introduction

44 Aerosol particles in the High Arctic atmosphere originate from a complex interplay of primary
45 and secondary emissions from oceanic, terrestrial, cryospheric, and anthropogenic sources,
46 followed by diverse atmospheric processes (Schmale et al., 2021). They play a crucial role in
47 the radiation balance, both directly by scattering and absorbing sunlight and indirectly by
48 influencing cloud formation and phase state through functioning as cloud condensation nuclei
49 (CCNs) and ice-nucleating particles (INPs) (Lohmann and Feichter, 2005; Penner et al., 2001;
50 Quinn et al., 2015; Yu et al., 2006). These effects are strongly governed by the particles' size
51 distribution and chemical composition (Dusek et al., 2006; Farmer et al., 2015; Kanji et al.,
52 2017; Pilinis et al., 1995).

53 The High Arctic predominantly consists of marine areas, characterized by a seasonally variable
54 extent of sea ice cover and open waters. Consequently, sea spray aerosol (SSA) particles
55 represent a key group of primary aerosol particles in this region (Heutte et al., 2025; Kang et
56 al., 2025; Schmale et al., 2022). As Arctic sea ice coverage continues to decline due to global
57 warming, enhanced by Arctic amplification (Cai et al., 2021; Francis and Wu, 2020; Wendisch
58 et al., 2017, 2023), larger expanses of open ocean are anticipated to become significant
59 sources of SSA emissions (Browse et al., 2014; Struthers et al., 2011). Although direct
60 measurements remain sparse, Sharma et al. (2019) readily observed increasing sea salt
61 aerosol production from sea spray over 34 years at the Arctic air chemistry observatory in
62 Alert, Canada.

63 SSA particles are generated through wind-driven wave action, which causes bubbles at the sea
64 surface to burst, ejecting film and jet droplets into the atmosphere (Veron, 2015). SSA
65 particles primarily consist of inorganic sea salt ions, mainly sodium and chloride, along with
66 organic matter (OM), including significant amounts of marine carbohydrates originating from
67 the sea surface microlayer (SML) and the underlying bulk seawater (Müller et al., 2010; van
68 Pinxteren et al., 2023; Quinn et al., 2015; Russell et al., 2010). In seawater, carbohydrates are
69 produced by both unicellular and multicellular organisms, predominantly as linear or
70 branched oligo- and polysaccharides (Aluwihare et al., 1997; Borch and Kirchman, 1997; Engel
71 and Händel, 2011; Khadem, 2012), collectively referred to as combined carbohydrates (CCHO).
72 They also exist as dissolved free carbohydrates (DFCHO), monosaccharides often rapidly



73 consumed by heterotrophic bacteria (Arnosti et al., 2021; Engel and Händel, 2011; Ittekkot et
 74 al., 1981; Kirchman et al., 2001).

75 Sodium in aerosol particles (Na^+_{aer}) is highly abundant in the marine boundary layer with only
 76 minor terrestrial sources and greater atmospheric stability compared to chloride (Cl^-_{aer}) (Chi
 77 et al., 2015; Keene et al., 1986; Manders et al., 2010; Sander et al., 2003). This makes it a
 78 valuable conservative tracer for studying the sea-to-air transfer and atmospheric
 79 transformation of organic compounds, including marine carbohydrates, as well as other
 80 inorganic SSA constituents. Notably, the ratio of OM to Na^+ is significantly higher in SSA
 81 particles than in seawater, reflecting not only the preferential enrichment of surface-active
 82 substances at the interface but also a more complex interplay of factors such as water
 83 solubility, biological activity within the ocean surface, and co-adsorption processes involving
 84 matrix constituents (Burrows et al., 2014; Gantt et al., 2011; Hasenecz et al., 2020, 2019;
 85 Hoffman and Duce, 1976; Jayarathne et al., 2016; van Pinxteren et al., 2017; Quinn et al., 2015;
 86 Russell et al., 2010; Schill et al., 2018). This enrichment is particularly pronounced in
 87 submicron particles compared to supermicron particles. Furthermore, following the sea-to-air
 88 transfer of OM and CCHO, recent laboratory (Hasenecz et al., 2020; Malfatti et al., 2019) and
 89 field (Zeppenfeld et al., 2021, 2023) observations suggest their molecular transformation or
 90 additional in-situ formation, driven by abiotic, microbial or enzymatic activities in the
 91 atmosphere.

92 SSA particles are known to function as both CCNs (Orellana et al., 2011; Xu et al., 2022) and
 93 INPs (Alpert et al., 2022; DeMott et al., 2016; Hill et al., 2023; Mirrieles et al., 2024),
 94 underscoring their important role in cloud microphysics, cloud formation, and precipitation
 95 processes. Recently, Hartmann et al. (2025) demonstrated, through a combination of lab and
 96 field data, that SSA particles' ice-nucleating activity is likely attributable to the polysaccharides
 97 they contain. Model simulations further indicated that the ice-nucleating activity of marine
 98 polysaccharides is particularly significant within the temperature range between -20 and -15°C
 99 in remote oceanic regions, where contributions from terrestrial INP sources are minimal or
 100 absent. Furthermore, Rocchi et al., (2024) demonstrated that the presence of glucose-rich
 101 CCHO, in combination with sea salt, significantly enhances SSA production in eastern Arctic
 102 waters. This finding may improve the predictability of SSA emissions in marine models.



103 In the field, marine combined carbohydrates in aerosol particles (CCHO_{aer}) have been
104 predominantly measured at ship-based or coastal locations, which are in close proximity to
105 local marine emission sources both horizontally and vertically (Leck et al., 2013; van Pinxteren
106 et al., 2023; Zeppenfeld et al., 2021, 2023). In contrast, only a few studies have investigated
107 CCHO_{aer} (Karl et al., 2019; Yttri et al., 2024) at an elevated mountain site in a marine-influenced
108 setting, aiming to assess atmospheric concentrations at higher altitudes. Vertically resolved
109 field data comparing ground-level and elevated altitudes using mobile platforms, however,
110 have been unavailable for marine CCHO_{aer} in the past. As a result, it remains unclear to what
111 extent and under which conditions CCHO_{aer} reach the upper marine boundary layer and the
112 free troposphere. This is due to several challenges, including low atmospheric concentrations
113 pushing the instruments' detection capabilities for offline analyses to their limits, the lack of
114 highly resolving online detection techniques for CCHO_{aer} , and in particular the absence of
115 lightweight yet powerful pumps with high flow rates. Additionally, the very short sampling
116 times typically available on mobile airborne measurement platforms pose a further obstacle
117 for measuring marine CCHO_{aer} in aerosol particles across altitudes within the troposphere. This
118 lack of vertical field data leaves high uncertainty about the broader relevance of these
119 biomolecules in cloud formation and glaciation beyond a controlled laboratory setup.

120 Previous airborne measurements around Svalbard (Hara et al., 2003) and the Canadian Arctic
121 (Köllner et al., 2017) demonstrated that SSA particles—identified by Na^+ and Cl^- —are present
122 in higher altitudes of the lower troposphere, and, to a lesser extent, reach the middle free
123 troposphere (3–6 km a.s.l.). Some of these aerosol particles showed signs of atmospheric
124 aging, such as the replacement of chloride with nitrate and sulfate in the SSA particles. While
125 vertically resolved data exists for major inorganic SSA constituents, such extended information
126 is lacking for marine CCHO_{aer} .

127 Recent methodological advances now allow for a more detailed investigation of the transport
128 mechanisms and atmospheric chemical fate of marine carbohydrates. In this study, we
129 present atmospheric concentrations of these biomolecules alongside common inorganic SSA
130 constituents. Measurements were conducted from ground level up to various altitudes within
131 the boundary layer and lower free troposphere using a tethered helium balloon in Ny-Ålesund
132 on Svalbard during autumn 2021 and spring 2022. For selected cases, we examined the
133 influence of mixing state, meteorological conditions, and air mass history on the observed
134 aerosol composition. Finally, this study addresses the potential atmospheric processing and



135 transformation of marine carbohydrates, with a focus on their possible contribution to
136 secondary aerosol formation and their implications for atmospheric chemistry and cloud-
137 relevant processes.



2. Experimental

2.1 Study area: Ny-Ålesund as an atmospheric observation site

Ny-Ålesund, located at 78.9°N at the Kongsfjorden in Svalbard (Norway), belongs to the world's northernmost permanently inhabited settlements with a year-round accessibility. It serves as a key research site for studying Arctic climate change and Arctic amplification. Ny-Ålesund hosts long-term monitoring sites for aerosols and meteorology, such as the Zeppelin Observatory (Platt et al., 2022), Gruvebadet (Amore et al., 2022), and the AWIPEV Observatory (Maturilli et al., 2013, 2015). These, along with additional research stations operated by various international institutions, provide valuable data for both long-term atmospheric studies and short-term investigations like the present one.

However, Ny-Ålesund is not representative of the entire High Arctic. Its distinct topography, situated within a fjord and surrounded by high mountains up to 800 m, leads to complex atmospheric dynamics, including foehn-like effects (Shestakova et al., 2021). The local boundary layer is relatively shallow characterized by an average mixing layer height below 700 m and a strong influence by orographic effects (Chang et al., 2017; Dekhtyareva et al., 2018; Gierens et al., 2020). While free-tropospheric winds are predominantly westerly, surface winds result from an interplay of land-sea breeze circulations, southeasterly channeled winds along the fjord axis, and katabatic flows from the Zeppelin mountain range, the Broeggerbreen glacier, or the Kongsvegen glacier (Esau and Repina, 2012; Gierens et al., 2020). Additionally, large wind shear has been observed to generate turbulence, leading to frequent neutral stratification (Gierens et al., 2020). Furthermore, boundary layer mixing can occur even when a positive gradient in potential temperature suggests a more stable stratification. During the present field campaign, we observed that near-surface winds often shift unpredictably, changing direction without a clear pattern, making airflow dynamics challenging to interpret.

From an oceanographic perspective, Svalbard is similarly exceptional. The region is influenced by the cold Arctic waters of the Spitsbergen Polar Current and the warm waters of the West Spitsbergen Current (Feltracco et al., 2021). Kongsfjorden, located on the western coast of Spitsbergen, lies at the interface of High Arctic and Atlantic influences, making it a dynamic and variable environment (Bischof et al., 2019).



Therefore, findings from Ny-Ålesund may not be fully transferable to atmospheric processes over sea ice or the open ocean in the High Arctic. However, in general, the representativeness of any single Arctic site is highly questionable, as Freud et al., (2017) found significant heterogeneity in aerosol particle size distribution across all Arctic sites in their study.

2.2 Field sampling

The field samples (aerosol particles, bulk seawater and SML) for this study were collected near Ny-Ålesund and from the adjacent Kongsfjorden during autumn 2021 and spring 2022.

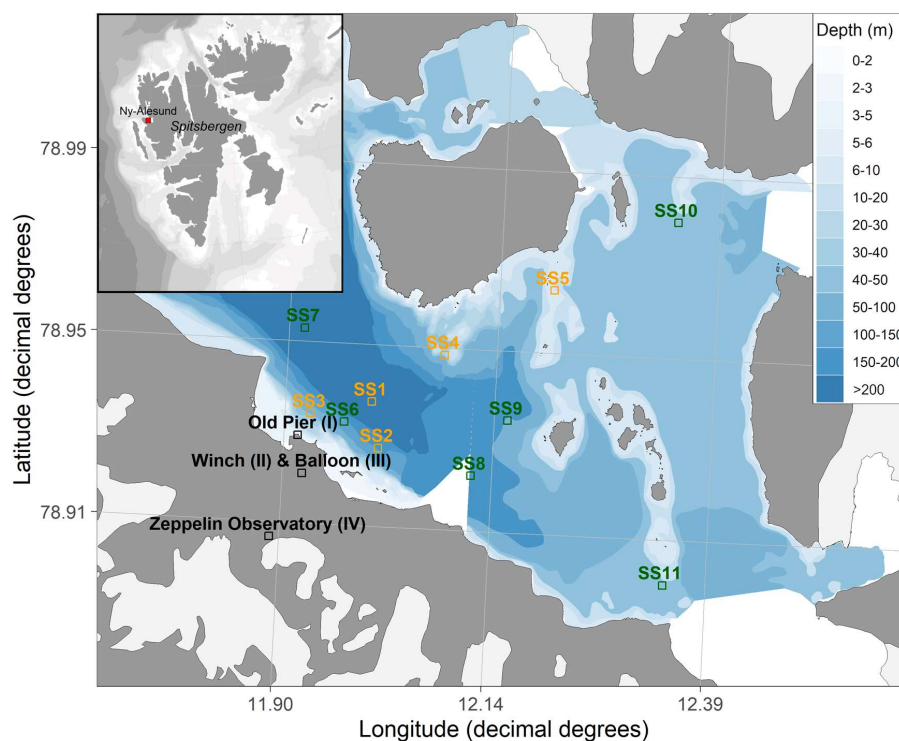


Figure 1. Map of the sampling locations. Aerosol particles were collected at: (I) the Old Pier, representing fresh SSA emissions; (II) the winch, representing ground measurements; (III) the tethered balloon at various altitudes; and (IV) the Zeppelin Observatory, serving as a reference for comparison. Bulk and SML samples were collected from different locations within Kongsfjorden. Orange squares (SS1-SS5) indicate autumn 2021 samples, while green squares (SS6-SS11) represent spring 2022 samples. Blue shading indicates water depth.



178 *a) Bulk seawater and SML sampling*

179 In total, 11 bulk surface seawater and 11 SML samples were taken from a small boat at various
 180 dates and locations across the Kongsfjorden (**Figure 1, Table S1**). Bulk water samples were
 181 obtained from a depth of 1 m using low-density polyethylene (LDPE) bottles secured to a
 182 telescopic rod. The corresponding SML samples were collected using the glass plate technique
 183 (Cunliffe and Wurl, 2014; van Pinxteren et al., 2012). A glass plate measuring
 184 50 cm × 20 cm × 0.5 cm, with an oval sampling area of 2000 cm², was immersed vertically into
 185 the surface of the fjord seawater and withdrawn at a steady rate of 15 cm s⁻¹. The SML film
 186 attached to the glass surface was drained into a precleaned wide-neck plastic bottle using a
 187 funnel and a framed Teflon wiper. Water samples were filtered through 0.2 µm polycarbonate
 188 filters (Whatman® Nuclepore™, 47 mm diameter) to separate dissolved and particulate
 189 fractions. The filtrate, filters and field blanks were preserved at -20°C until chemical analyses
 190 (inorganic ions, carbohydrates). Sea surface temperature (SST) was measured directly from
 191 the boat at a depth of approximately 10 cm using a digital thermometer.

192 *b) Aerosol particle sampling in the surroundings of Ny-Ålesund*

193 Total suspended aerosol particles (TSP) were captured on polycarbonate filters (0.8 µm,
 194 Whatman® Nuclepore™, 47 mm diameter) at four locations (**Figure 1**): (I) Near the Old Pier
 195 next to Kongsfjorden (8 samples), representing fresh SSA emissions; (II) near the balloon winch
 196 close to the AWIPEV Observatory (17 samples), representing ground measurements; (III) at
 197 high altitudes at the tethered balloon (14 samples); and (IV) at the Zeppelin Observatory
 198 (1 sample), serving as a reference for comparison. **Table S2** provides details of individual
 199 aerosol particle samplings near the Old Pier (I), while **Table S3** presents the sampling times,
 200 locations and heights of all the individual high-altitude aerosol samples (III & IV), along with
 201 the corresponding simultaneous ground-level samples (II) taken near the winch.

202 For sampling aerosol particles at the Old Pier (4 m above sea level), a filter holder with a
 203 polycarbonate filter attached to a pump was used. Sampling lasted between 4 and 7 days.
 204 Flow rates, measured at the beginning and the ending of the sampling with a flowmeter,
 205 ranged from 5 to 10 L min⁻¹, with total air volumes between 44 and 82 m³. The estimated
 206 diameter-dependent collection efficiency of this TSP sampling setup, assuming a 90°
 207 aspiration angle, is shown in **Figure S1**. To reduce the risk of pump failure due to cold
 208 temperatures or snow, the pumps were housed in a Zarges box for protection.



High-altitude TSP samples were collected using the helium-filled tethered balloon BELUGA, as described in detail by Pilz et al. (2023). The balloon's altitude was controlled using an electric winch located near the AWIPEV Observatory, with ascent and descent rates from 1 to 3 m s⁻¹. The tethered balloon operated under various meteorological conditions, including both clear and cloudy skies. At a specified altitude, a HALFBAC (High-volume And Light-weight Filter sampler for BALloon-borne appliCation) (Grawe et al., 2023) collected aerosol particles 2-3 m below the balloon. The HALFBAC is a custom-designed, lightweight aerosol particle sampler operating at a pump flow between 25 and 35 L min⁻¹. It is capable of collecting sufficient aerosol mass on filters at high altitudes for subsequent offline chemical and microphysical analyses. Simultaneously, another HALFBAC collected ground-level aerosol particles near the electric winch (20 m above sea level). Additionally, one aerosol sample (Filter ID 62, sampling date: 10/05/2022) was collected at the Zeppelin Observatory, a permanent monitoring station located at 474 m a.s.l. on Zeppelinfjellet, using the HALFBAC. Synchronized aerosol particle sampling at the winch and the balloon typically lasted around two hours, as detailed in **Table S3**. The collection efficiency for TSP sampling using HALFBAC is discussed in the supplement (A1) and **Figure S1**.

225

2.3 Chemical analyses from offline aerosol particle filters and seawater

For the analysis of major cations, anions and marine carbohydrates in aerosol particles, the complete polycarbonate filters were extracted in 6-7 mL of ultrapure water (resistivity > 18.2 MΩ) for two hours followed by a filtration through a 0.45 μm syringe filter. Frozen seawater samples were gently thawed at 4°C one day before analysis.

a) Major cations and anions

Major inorganic ions, including sodium (Na⁺), potassium (K⁺), magnesium (Mg²⁺), calcium (Ca²⁺), chloride (Cl⁻), sulfate (SO₄²⁻), and oxalate, were quantified in 0.45 μm filtered aqueous aerosol extracts, bulk seawater and SML samples using ion chromatography (Dionex ICS-6000, Thermo Scientific) as described by Zeppenfeld et al. (2021). Cations were separated isocratically with a 36 mM methanesulfonic acid eluent on a Dionex IonPac CS16-4 μm column (2 mm × 250 mm), paired with a Dionex IonPac CG16-4 μm guard column (2 mm × 50 mm). For anion separation, a gradient from 4 to 40 mM KOH was applied on a Dionex IonPac AS18



239 column (2 mm × 250 mm), along with a Dionex IonPac AG18 guard column (2 mm × 50 mm).
 240 The analytical uncertainty for each ion was below 5%. Aerosol extracts were measured
 241 undiluted, while bulk seawater and SML samples were analyzed at a 1:15,000 dilution.

242

243 *b) Dissolved free and combined carbohydrates*

244 Carbohydrates in seawater and aerosol particle extracts were measured according to the
 245 protocols outlined by Zeppenfeld et al. (2020, 2021), utilizing high-performance anion-
 246 exchange chromatography with pulsed amperometric detection. The system was equipped
 247 with a Dionex CarboPac PA20 analytical column (3 mm × 150 mm) and a Dionex CarboPac
 248 PA20 guard column (3 mm × 30 mm). The applied eluent gradient separated the following
 249 monosaccharide units: fucose (Fuc), rhamnose (Rha), arabinose (Ara), galactose (Gal), glucose
 250 (Glc), xylose (Xyl), mannose (Man), fructose (Fru), galactosamine (GalN), glucosamine (GlcN),
 251 muramic acid (MurAc), galacturonic acid (GalAc), and glucuronic acid (GlcAc). The analytical
 252 uncertainty for each monosaccharide was below 10%. dFCHO represents the total of
 253 identifiable free monosaccharides, whereas CCHO include only those monosaccharides
 254 released through acid hydrolysis (0.8 M HCl, 100°C, 20 h). For seawater samples, particulate
 255 combined carbohydrates (pCCHO, >0.2 µm) were measured from 0.2 µm polycarbonate
 256 filters, while dissolved combined carbohydrates (dCCHO, <0.2 µm) were measured from the
 257 filtrate after desalination via electrodialysis. Both fractions were later summed to represent
 258 the total CCHO.

259

260 **2.4 Vertical profiles from online measurements**

261 *a) Size-resolved aerosol particles number concentrations*

262 An optical particles size spectrometer (POPS, Handix), integrated into the Cubic Aerosol
 263 Measurement Platform (CAMP) as described by Pilz et al. (2022), provided the integrated total
 264 number concentrations (N_{150}) for aerosol particles between 150 and 2900 nm at a temporal
 265 resolution of 1 second. On selected dates of HALFBAC sampling, CAMP was operated
 266 simultaneously 25 m below the balloon providing insight into the vertical profile of N_{150} during
 267 specific events. Vertical profiles are presented as rolling averages over 30 seconds.

268

269



270 *b) Meteorological observations and calculations*

271 Standard meteorological parameters—including altitude, ambient temperature (T), wind
 272 speed (U), wind direction, air pressure (p), and relative humidity (RH)—were measured for the
 273 elevated-altitude samples using a standard meteorology package positioned approximately
 274 20 m below the balloon (Pilz et al., 2023). The potential temperature (θ) within the
 275 atmospheric column - as a measure of the static stability of the unsaturated atmosphere - was
 276 calculated using Eq. I, where T is the ambient temperature (K), p is the atmospheric pressure
 277 (hPa), p_0 is the reference pressure (1000 hPa), R is the specific gas constant ($287 \text{ J kg}^{-1} \text{ K}^{-1}$) and
 278 c_p is the specific heat capacity of dry air at constant pressure ($1004 \text{ J kg}^{-1} \text{ K}^{-1}$).

$$279 \quad \theta = T \left(\frac{p_0}{p} \right)^{\frac{R}{c_p}} \quad (\text{Eq. I})$$

280 Specific humidity (q)—remaining constant during adiabatic ascent or descent as long as no
 281 phase changes occur—was calculated using Eq. II from Egerer et al. (2021), where R_d/R_v (the
 282 ratio of specific gas constants for dry air and water vapor) is approximately 0.622, and $e_s(T)$
 283 represents the temperature-dependent saturation vapor pressure.

$$284 \quad q = \frac{R_d/R_v \cdot e_s(T) \cdot RH}{p - (1 - R_d/R_v) \cdot e_s(T) \cdot RH} \quad (\text{Eq. II})$$

285 Meteorological data measured 2 m above the ground (13 m above sea level) at the AWIPEV
 286 Atmospheric Observatory (Maturilli, 2020), represented the weather conditions during
 287 aerosol sampling at the winch.



2.5 Supporting observations and model calculations

Major inorganic ions measured at the Zeppelin Observatory with a 24-hour resolution using a statically installed aerosol sampler (Filter_3pack) as part of the European Monitoring and Evaluation Programme (Tørseth et al., 2012) by the Norwegian Polar Institute (NPI) and the Norwegian Institute for Air Research (NILU) were obtained from the EBAS database for the study duration (Aas et al., 2022, 2023). The Filter_3pack data were utilized in two ways:

1. **Comparing sampling techniques:** Data from the Filter_3pack were compared with one HALFBAC aerosol particle sample collected directly at the Zeppelin Observatory (Filter ID 62, 10/05/2022) to evaluate potential artifacts arising from differences in sampling techniques and filter media. Despite variations in time resolution and methods, sodium, potassium, chloride, and sulfate concentrations showed strong agreement (detailed in the supplement A2 and **Figure S2**).
2. **Comparison with balloon data:** Sodium concentrations measured at the Zeppelin Observatory were directly compared with those obtained from the tethered balloon sampling.

Information on the occurrence of clouds and hydrometeor types at Ny-Ålesund were taken from the Cloudnet classification product (Illingworth et al., 2007; Nomokonova et al., 2019), which is based on a combination of ground-based cloud radar, ceilometer, and numerical weather prediction output. Vertically integrated ice water content (IWC), i.e. ice water path (IWP) has been calculated from the Cloudnet IWC product following Hogan et al. (2006). Vertically integrated cloud liquid water (liquid water path; LWP) and water vapor (IWV) were taken from zenith HATPRO microwave radiometer measurements (Nomokonova et al., 2019).

The 48-hour back-trajectories for the aerosol sampling periods were generated using the NOAA HYSPLIT model (Stein et al., 2015). Trajectories were calculated hourly based on GDAS1 meteorological data (Global Data Assimilation System; 1° spatial resolution; 3-hour intervals) for various arrival heights: 50 m (ground level), 474 m (Zeppelin Observatory), and the specific balloon sampling altitudes. Sea ice concentration data were obtained from the NOAA-maintained ERDDAP server (Environmental Research Division's Data Access Program). The back-trajectories were used to assess the relative influence of distant sources, such as the marginal ice zone, versus local ice-free oceanic emissions on the aerosol chemical composition. Given the rather short atmospheric residence times of SSA particles—typically



319 less than two days for supermicron particles (Madry et al., 2011; Veron, 2015), which account
 320 for most of the SSA mass —and the increasing uncertainties associated with longer back-
 321 trajectory periods, we consider 48 hours back-trajectory length appropriate for this analysis.

322 Ocean surface concentrations for total chlorophyll a (TChl- a) and dissolved acidic
 323 polysaccharides were obtained by a coupled setup of the ocean sea ice biogeochemistry
 324 model FESOM2.1-REcoM3 (Gürses et al., 2023), to which additional state equations have been
 325 added to simulate dissolved and particulate organic carbon following Engel et al. (2004) and
 326 Schartau et al. (2007). The simulation was set up following Gürses et al. (2023) and using the
 327 Arctic-specific tuning of Oziel et al. (2022). Monthly model output was obtained on an irregular
 328 grid with approximately 4.5 km resolution in the Arctic Ocean. This configuration has already
 329 been applied successfully in Leon-Marcos et al. (2025).

330

331 **2.6 Statistics, data processing, visualization and text optimization**

332 Statistical analyses, calculations and visualization were conducted using OriginPro 2024,
 333 Microsoft Excel, IDL, python3 and R version 4.2.1 with the ncdf4 (Pierce, 2023), openair
 334 (Carslaw and Ropkins, 2012), reshape2 (Wickham, 2007), scales (Wickham et al., 2023b),
 335 lubridate (Grolemund and Wickham, 2011), cmocean (Thyng et al., 2016), maps (Brownrigg,
 336 2023), mapdata (Brownrigg, 2013), rgdal (Bivand et al., 2022), raster (Hijmans, 2023),
 337 RColorBrewer (Neuwirth, 2022), sp (Bivand et al., 2013), dplyr (Wickham et al., 2023a), ggplot2
 338 (Wickham, 2016), and PlotSvalbard (Vihtakari, 2020) packages. Box-and-whisker plots
 339 illustrate the interquartile range (box), the median (horizontal line inside the box), the mean
 340 (open square), the minimum and maximum values (whiskers). Text and language were
 341 optimized using Open AI's ChatGPT-4 Turbo.



3. Results and Discussion

3.1 Chemical constituents in marine aerosol particles from their oceanic source to elevated altitudes

Sodium in aerosol particles (Na^+_{aer})

Sodium, a dominant and chemically stable component of SSA, is commonly used as a tracer for tracking ocean-derived emissions in atmospheric studies (Manders et al., 2010; van Pinxteren et al., 2017; White, 2008). In this study, consistently high Na^+_{aer} concentrations were observed on the TSP filters at the Old Pier next to Kongsfjorden in both autumn 2021 and spring 2022 (**Figure 2a**), ranging from 140 to 1470 ng m^{-3} (median: 495 ng m^{-3} ; $n=8$). During the campaign, sea ice coverage in Kongsfjorden varied; however, significant areas around Ny-Ålesund—particularly near the Old Pier—remained ice-free, suggesting that local sea ice likely had only little influence on sea spray emissions.

Na^+_{aer} concentrations measured at the winch site, located further inland but still at ground level (35–3710 ng m^{-3} ; median: 155 ng m^{-3} ; $n=17$), and in elevated HALFBAC samples between 321 and 1112 m (23–850 ng m^{-3} ; median: 124 ng m^{-3} ; $n=15$) were generally lower in both minimum and median values compared to those at the Old Pier. Nevertheless, occasional high concentration events were observed across all three sampling locations. The large variability in Na^+_{aer} concentrations, ranging from the lower ng m^{-3} to a few $\mu\text{g m}^{-3}$, aligns with other marine sampling locations and altitudes (Fomba et al., 2014; Li et al., 2024; Ooki et al., 2002; Theodosi et al., 2010; Triesch et al., 2021; Zeppenfeld et al., 2021, 2023).

Since aerosol particle sampling at the winch and the balloon was always synchronized, direct comparisons between the two sites were possible. Several events showed nearly identical sodium concentrations at both locations (e.g., 30 September: 191 ng m^{-3} at the winch and 207 ng m^{-3} at the balloon; 2 October: 35 ng m^{-3} at the winch and 36 ng m^{-3} at the balloon; 9 October: 59 ng m^{-3} at the winch and 60 ng m^{-3} at the balloon; 12 November: 240 ng m^{-3} at the winch and 223 ng m^{-3} at the balloon). In contrast, other dates revealed significant differences, with much lower concentrations at higher altitudes than at the ground (e.g., 27 September: 1840 ng m^{-3} at the winch and 23 ng m^{-3} at the balloon; 5 April: 84 ng m^{-3} at the winch and 54 ng m^{-3} at the balloon; 11 May: 496 ng m^{-3} at the winch and 125 ng m^{-3} at the balloon), but also two instances of even higher concentrations recorded at the balloon (24



372 September: 47 ng m⁻³ at the winch and 99 ng m⁻³ at the balloon; 3 April: 77 ng m⁻³ at the winch
373 and 194 ng m⁻³ at the balloon). These variations can likely be attributed to atmospheric
374 depletion processes, including dry and wet deposition (Farmer et al., 2021), atmospheric
375 dilution during vertical and horizontal transport from the emission region (Wong et al., 2019),
376 vertical mixing conditions (Pilz et al., 2024) and differences in air mass histories (Willis et al.,
377 2018). The influence of atmospheric meteorological conditions on the vertical distribution of
378 chemical compounds will be analyzed and discussed in detail for three selected cases later in
379 this study.

380 Concentrations measured at the Zeppelin Observatory, where Na⁺_{aer} is routinely monitored,
381 were largely consistent with those observed in the balloon samples, showing an overall
382 agreement ranging between 56 and 213%, with five events demonstrating excellent
383 agreement of 92–107% (**Table S6**). This similarity is remarkable considering the differences in
384 sampling time resolution (24 h at Zeppelin vs. 1–2 h for the balloon), sampling altitudes, the
385 horizontal distance between the sites, the complex topography of Svalbard (Gierens et al.,
386 2020; Shestakova et al., 2021), and the fact that meteorological conditions and atmospheric
387 mixing states have not yet been considered. Up to 1100 m altitude, encompassing both the
388 boundary layer and the free troposphere, sodium was detectable and quantifiable, sometimes
389 at concentrations comparable to those near the emission source. This indicates that SSA
390 compounds are either effectively mixed throughout the vertical atmospheric column, or reach
391 heights relevant for cloud formation through advection. Such observations are consistent with
392 aircraft-based sodium measurements reported by Hara et al. (2003) and Köllner et al. (2017).

393 The longer SSA particles remain in the atmosphere, the greater their exposure to atmospheric
394 aging processes, which can alter their impact on cloud formation. While Na⁺_{aer} in SSA is
395 considered chemically stable, co-emitted OM including carbohydrates may undergo physical,
396 chemical and microbial transformations, as suggested by Zeppenfeld et al. (2021, 2023). This
397 aspect will be explored further in the following sections.

398

399

400

401

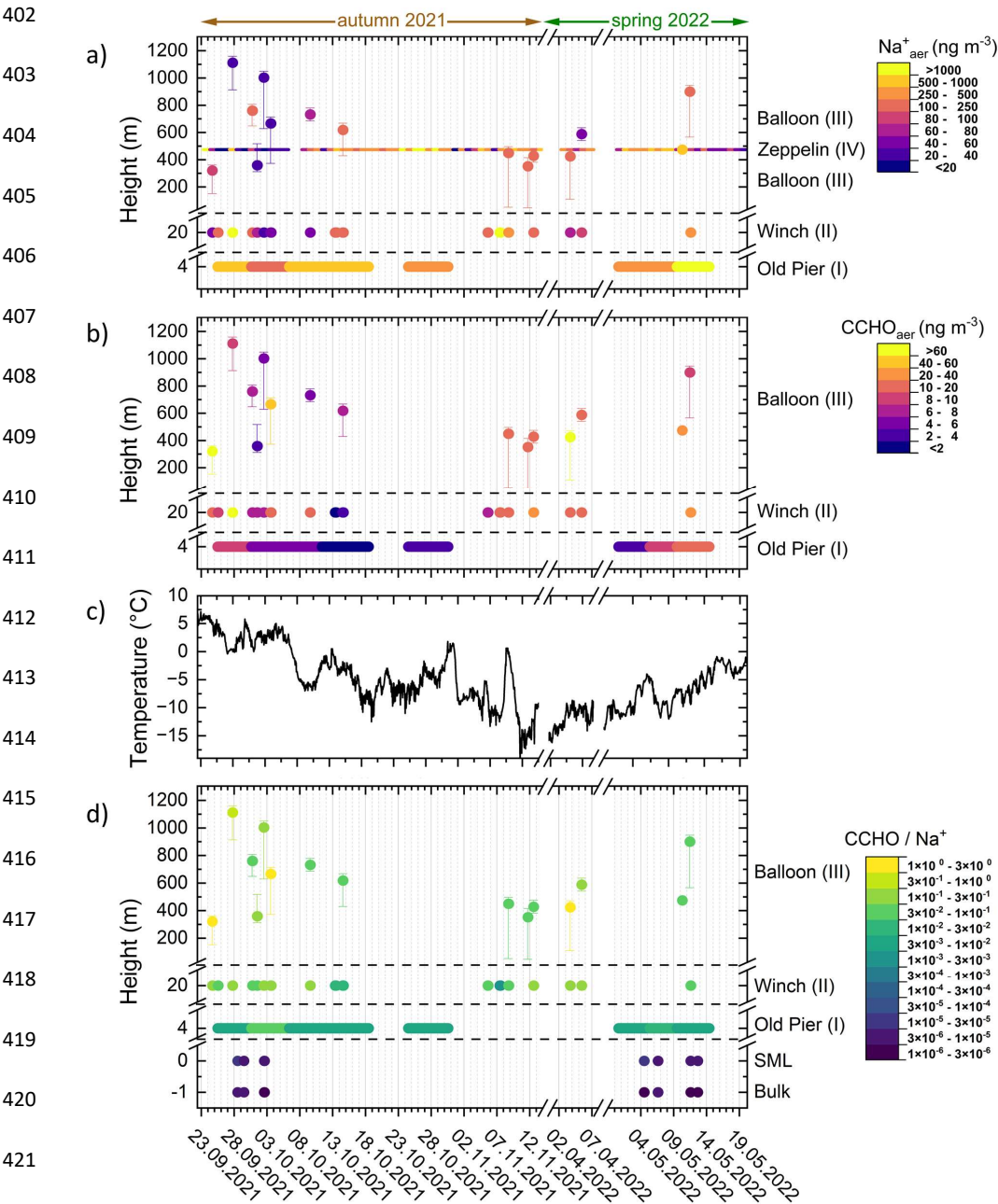


Figure 2. Time-resolved atmospheric concentrations of a) sodium and b) CCHO_{aer} in aerosol particles (TSP) collected in autumn 2021 and spring 2022 in Ny-Ålesund at several heights (m a.s.l.) from four sites: Old Pier, winch near the AWIPEV Observatory, balloon and the Zeppelin Observatory. Dots represent the median height during the total sampling time and vertical error bars represent maximum and minimum height of the sampler during the active sampling. The x-axis ticks represent the start of each date at midnight. c) Air temperature (2 m above ground) measured at the AWIPEV Observatory. d) CCHO/Na^+ ratios within the bulk seawater, the SML and in the aerosol particles at several heights.



426 ***Combined carbohydrates in fresh SSA and their oceanic origin***

427 Similar to sodium, CCHO_{aer} were detected in all atmospheric samples across all sites and
 428 altitudes (**Figure 2b**). At the Old Pier, CCHO_{aer} concentrations ranged from 1.6 to 10.0 ng m⁻³
 429 (median: 5.0 ng m⁻³; n=8). A seasonal pattern emerged, with the highest values observed at
 430 the beginning (September 2021) and end (May 2022) of the study period, while lower
 431 concentrations were recorded during the colder, darker months in between (**Figure 2c**).
 432 However, it should be noted that no aerosol samples were collected during the coldest winter
 433 months.

434 The seasonal variation of CCHO_{aer} at the Old Pier may be linked to the seasonal dynamics of
 435 marine CCHO in the surface water of Kongsfjorden, their most probable local emission source
 436 for SSA. These dynamics are likely driven by seasonal shifts in phytoplankton composition as
 437 well as overall primary production (Assmy et al., 2023; Mayot et al., 2018). Reduced or absent
 438 production in Kongsfjorden during the winter and early spring, as indicated by low
 439 phytoplankton and TChl-a concentrations, contrasts with significantly higher values from mid-
 440 spring to mid-autumn (van de Poll et al., 2021).

441 Similar seasonality was observed for selected monosaccharides among the dissolved
 442 combined carbohydrates (dCCHO) in Kongsfjorden seawater, the primary source of
 443 atmospheric CCHO_{aer}. In particular, fucose, galactosamine, and rhamnose in bulk water dCCHO
 444 exhibited a distinct pattern, closely following SST. Their concentrations peaked in late
 445 September/early October, while being much lower (44-67%) in early to mid-May (**Figure S3**).
 446 However, this trend was less pronounced for glucose in bulk water dCCHO and even weaker
 447 in the SML across most monosaccharide units (**Figure S3**).

448 In contrast, particulate combined carbohydrates (pCCHO)—including contributions from
 449 transparent exopolymer particles (TEPs), detritus, and dead or living cells—showed no clear
 450 seasonal trend in seawater (**Figure S4**). While dCCHO in bulk water exhibited relatively low
 451 spatial and intra-seasonal variability, pCCHO and SML samples were considerably more
 452 variable among all samples, even among samples from the same season (**Figure S5**). This
 453 variability likely reflects pCCHO's rapid dynamics in relation to phytoplankton blooms (Becker
 454 et al., 2020; Engel et al., 2012; Fabiano et al., 1993). Additional drivers include the
 455 spontaneous formation of TEPs from dCCHO precursors in turbulent waters, as well as the



vertical transport of pCCHO through sedimentation (e.g., as marine snow) or its accumulation in the SML depending on its buoyancy (Burns et al., 2019; Engel, 2004; Robinson et al., 2019b, a; Wurl and Holmes, 2008). The SML, in particular, may be more sensitive to these dynamics than the more stable bulk water, potentially explaining the greater fluctuations.

On the other hand, dCCHO measured in bulk water—similar to dissolved organic carbon (Hansell, 2013; Keene et al., 2017)—may be generally dominated by recalcitrant and semi-recalcitrant compounds. The labile fraction of dCCHOs is likely more rapidly consumed by heterotrophic bacteria (Goldberg et al., 2011) and the remaining dCCHOs presumably represent substrates that are less available to microbial metabolism. Notably, combined glucose showed high variability in both dCCHO and pCCHO, likely due being the main constituent of abundant storage macromolecules such as laminarin (Becker et al., 2020) during periods of photosynthetic overflow (Barthelmeß et al., 2025), as well as its relatively rapid microbial utilization (Kharbush et al., 2020). In conclusion, the seasonal variation of CCHO_{aer} aligns with the observed seasonality of certain marine carbohydrates in the Kongsfjorden, indicating that dCCHO in surface seawater may be the major origin of freshly emitted CCHO_{aer}.

CCHO_{aer} at the winch and higher altitudes

CCHO_{aer} concentrations were also measured at the winch site (1.9–194 ng m⁻³; median: 10.6 ng m⁻³; n=17) and at the balloon (3.8–274 ng m⁻³; median: 10.2 ng m⁻³; n=15), showing a broader range and significantly higher median and maximum values compared to the Old Pier. The higher concentrations, found more inland and at higher altitudes, compared to the Old Pier were unexpected and suggest sources beyond an exclusive primary sea-air transfer, which will be discussed below. Unlike the Old Pier samples, no clear seasonal pattern was evident in these locations, nor was there any apparent dependence on sampling height. The lacking seasonality at the Winch site, unlike at the Old Pier, may be due to its more inland position, making it more sensitive to wind direction and changing weather. Also, the higher temporal resolution of the samples likely captured short-term fluctuations rather than integrated seasonal trends. In addition, atmospheric processing during transport and the lack of true winter samples may have further obscured any clear seasonal signal.



485 Similar to sodium, certain events showed comparable CCHO_{aer} concentrations between the
 486 winch and balloon samples (e.g., 30 September: 6.5 ng m⁻³ at the winch and 8.0 ng m⁻³ at the
 487 balloon; 2 October: 6.3 ng m⁻³ at the winch and 5.8 ng m⁻³ at the balloon; 8 November:
 488 11.1 ng m⁻³ at the winch and 10.2 ng m⁻³ at the balloon; 12 November: 26 ng m⁻³ at the winch
 489 and 17 ng m⁻³ at the balloon). On other dates, however, CCHO_{aer} concentrations were
 490 markedly lower at higher altitudes (e.g., 27 September: 194 ng m⁻³ at the winch and 8.6 ng m⁻³
 491 at the balloon; 11 May: 25 ng m⁻³ at the winch and 8.1 ng m⁻³ at the balloon). Interestingly,
 492 there were also instances where CCHO_{aer} concentrations were much higher at elevated
 493 altitudes than at ground level (e.g., 24 September: 10.2 ng m⁻³ at the winch and 136 ng m⁻³ at
 494 the balloon; 3 April: 15.9 ng m⁻³ at the winch and 275 ng m⁻³ at the balloon). In most cases,
 495 CCHO_{aer} covaried with sodium. However, a notable exception occurred on 3 October, when
 496 Na⁺_{aer} concentrations were slightly lower at the balloon (35 ng m⁻³) than at the ground
 497 (54 ng m⁻³), whereas CCHO_{aer} showed the opposite pattern, with higher concentrations at the
 498 balloon (42 ng m⁻³) than at the winch (14 ng m⁻³).

499 To investigate the emission processes from the ocean and the atmospheric fate of marine
 500 CCHO, CCHO/Na⁺ ratios were calculated for all aerosol particle, bulk seawater and SML
 501 samples representing the primary sources of the SSA particle constituents studied here
 502 (**Figure 2d**). The lowest ratios, with minimal CCHO/Na⁺ variability, were observed in bulk
 503 seawater (2.0×10^{-6} to 6.0×10^{-6}). Slightly higher ratios were found in the SML (3.3×10^{-6} to
 504 2.5×10^{-5}), which can be explained with the known enrichment of CCHO in the SML compared
 505 to bulk seawater. Specifically, the enrichment factors (EF_{SML}) ranged between 1.3 and 4.1 for
 506 dCCHO and between 0.9 and 6.8 for pCCHO (**Figure S5**), which aligns well with the typical
 507 single-digit and occasionally two-digit enrichment factors reported in previous studies (Engel
 508 and Galgani, 2016; Gao et al., 2012; Zäncker et al., 2021; Zeppenfeld et al., 2021, 2023).

509 At the Old Pier, where fresh SSA was sampled, the ratios were significantly higher, ranging
 510 from 6.2×10^{-3} to 3.3×10^{-2} . This pronounced enrichment of CCHO relative to sodium in SSA
 511 particles compared to seawater has been discussed previously and is attributed to a chemo-
 512 selective sea-air transfer (Hasenecz et al., 2020, 2019; Jayarathne et al., 2016; Schill et al.,
 513 2018; Zeppenfeld et al., 2021, 2023). This process preferentially transfers surface-active
 514 organics during bubble bursting to the atmosphere, while highly water-soluble inorganic ions
 515 of the sea salt remain in the seawater. The enrichment effect is typically more pronounced in
 516 submicron particles, which have a higher relative contribution of organics than inorganic ions



517 (Quinn et al., 2015). In contrast, supermicron particles are predominantly composed of sea
 518 salts, although organic substances are still notably enriched compared to the surface
 519 seawater. Since this study measured total suspended particles, and the majority of SSA
 520 particle mass typically resides in the supermicron size range (Facchini et al., 2008; O'Dowd et
 521 al., 1997), our results could be considered more representative of supermicron aerosol
 522 particles.

523 At the winch sampling station, located at ground level but further inland, the CCHO/Na⁺ ratios
 524 within TSP aerosol particles ranged from 2.9×10^{-3} to 2.6×10^{-1} , being either similar to or
 525 slightly higher than those at the Old Pier. In contrast, balloon samples from elevated altitudes
 526 showed higher CCHO/Na⁺ ratios, ranging from 3.9×10^{-2} to 1.4×10^0 . This increase possibly
 527 results from the depletion of larger, salt-dominated supermicron SSA particles through dry
 528 and wet deposition (Croft et al., 2009; Hoppel et al., 2002; O'Dowd and de Leeuw, 2007),
 529 leading to a relatively greater contribution of OM-dominated submicron particles during
 530 transport and with extended atmospheric residence time. Furthermore, the increasing
 531 absolute concentration of CCHO at higher altitudes (**Figure 2b**) suggests an atmospheric
 532 formation process contributing to the elevated CCHO/Na⁺ ratios, potentially linked to
 533 microbial activity in the atmosphere, as discussed in detail in section 3.3.

534 The CCHO/Na⁺ ratios observed at the Old Pier and the Winch closely align with ship-based
 535 measurements in the High Arctic during the PASCAL cruise (2×10^{-3} to 2×10^{-1} for PM₁₀ from
 536 summed Berner impactor stages) conducted in May–July 2017 (Zeppenfeld et al., 2023). In
 537 contrast, the very high CCHO/Na⁺ values ($>1 \times 10^0$) observed at some elevated altitudes in this
 538 study were reported only occasionally for submicron particles (0.14–0.42 μm) during PASCAL.
 539 This may support the idea that supermicron particle deposition caused the shift in balloon
 540 sample ratios, though microbial contributions in the atmosphere are also possible. Moreover,
 541 these ratios far exceed those from the Southern Ocean near the western Antarctic Peninsula
 542 (8×10^{-4} to 7×10^{-3}) (Zeppenfeld et al., 2021), likely due to differences in surface seawater
 543 productivity.

544 Overall, it can be concluded that both Na⁺ and CCHO_{aer} are transported from the marine
 545 emission source to elevated heights within the lower troposphere. However, with longer
 546 atmospheric residence times, the chemical composition of aerosol particles appears
 547 increasingly altered in certain samples. As a key factor influencing these observations, the role



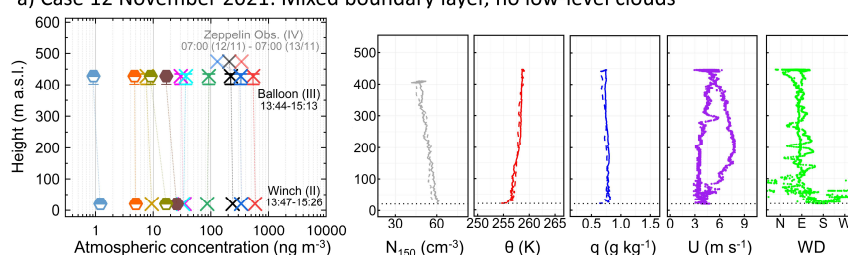
548 of meteorological conditions and atmospheric mixing in linking ground and balloon samples
549 will be discussed in the next section.



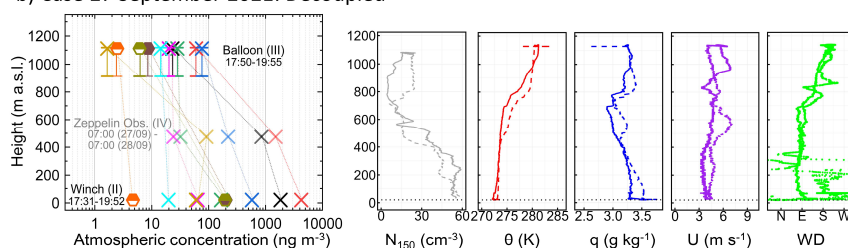
3.2 Impact of meteorological conditions on SSA particle constituents in higher altitudes

To examine how meteorological conditions and atmospheric mixing influenced Na^+_{aer} and CCHO_{aer} at elevated altitudes, three distinct cases with distinct, unvarying constant weather conditions were selected (**Figure 3**). These conditions allow for a detailed interpretation of the observed chemical values.

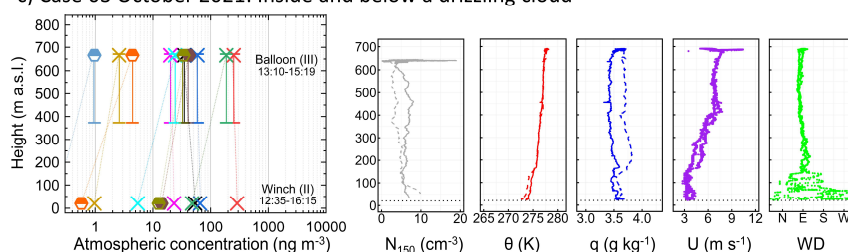
a) Case 12 November 2021: Mixed boundary layer, no low-level clouds



b) Case 27 September 2021: Decoupled



c) Case 03 October 2021: Inside and below a drizzling cloud



Legend: \times Na^+ \times Cl^- \times SO_4^{2-} \times Ca^{2+}
 \times K^+ \times Mg^{2+} \times oxalate \bullet CCHO
 \bullet Glc_{CCHO} \bullet Xyl_{CCHO} \bullet Ara_{CCHO}

Figure 3. Vertical profiles of three atmospheric cases showing mass concentrations of chemical constituents (inorganic ions, oxalate, total CCHO_{aer} , and major monosaccharides within CCHO_{aer}) in aerosol particles, measured on the ground (winch) and aloft (balloon) using offline filters. Vertical error bars indicate the range between minimal and maximal heights during active sampling at the balloon, while the symbols denote the median sampling heights. Data from the Zeppelin Observatory are also included when available and above detection limits, albeit with a 24-hour resolution. Dotted lines are included to aid in reading the vertical distribution of individual chemical substances. These profiles are complemented by aerosol particle number concentrations of particles bigger than 150 nm (N_{150}), potential temperature (θ), specific humidity (q), wind speed (U), and wind direction (WD) measured during the ascents (solid lines) and descents (dashed lines) of the balloon.



To assess atmospheric stability and layering in these cases, vertical profiles of potential temperature were utilized. To further confirm aerosol mixing conditions, additional meteorological parameters (specific humidity, wind speed and direction), vertical aerosol particle number concentrations of particles larger than 150 nm (N_{150}) (Figure 3), cloud conditions (Figure S6) and back-trajectory analyses (Figure 4) were considered. The selected cases include (a) a cloud-free mixed boundary layer (12 November 2021), (b) a free troposphere decoupled from the ground (27 September 2021), and (c) a boundary layer capped by precipitating clouds (03 October 2021).

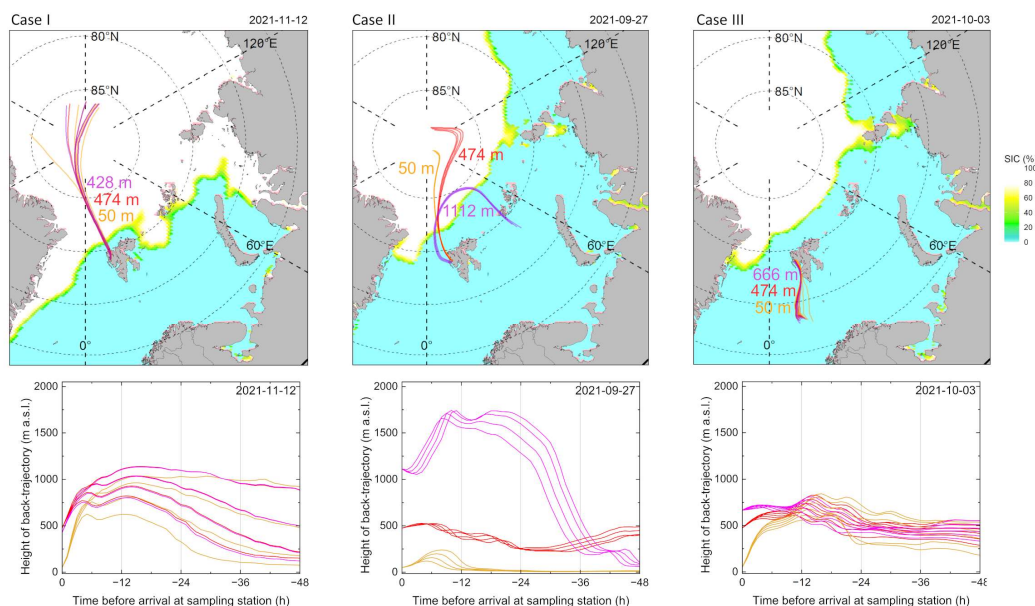


Figure 4. 48-hour back-trajectories calculated on an hourly basis for three arrival heights: orange (50 m, ground-level air masses), red (474 m, height of the Zeppelin Observatory), and purple (variable arrival height, high-altitude air masses sampled at tethered balloon). These are accompanied by daily sea ice concentration (SIC) maps (top) and height profiles (bottom) for three selected aerosol particle sampling cases.

Case I: Mixed boundary layer & no low-level clouds

On 12 November 2021, during the polar night, two HALFBACs were simultaneously operated at the ground and the balloon (median altitude of 428 m) for approximately 90 minutes. During active sampling at the ground, the average temperature was -16.7°C with a relative humidity of 69% and a wind speed of 1.5 m s^{-1} mostly from the southwest. At the balloon, sampling occurred at a similar average temperature of -17.5°C , a relative humidity of 72%, but a higher wind speed of 4.3 m s^{-1} from the northeast and southeast. With an IWV of less than 3 kg m^{-2} , the atmosphere was in general very dry (Figure S6a). The sky near the balloon was



572 clear of low-level clouds, with only a very thin mixed-phase cloud layer from 4.5 to 5 km
 573 altitude with insignificant LWP and IWP values (**Figure S6a**). While these clouds may have had
 574 some radiative effects, they were not expected to influence aerosol chemistry measurements
 575 within the boundary layer.

576 During the balloon's ascent to the aerosol sampling height, potential temperature increased
 577 from 255 K to 258 K, with the strongest gradient near the surface. Together with the wind
 578 speed profile, this allowed to estimate the surface mixing layer height using the Richardson
 579 number approach (Akansu et al., 2023), resulting in a very low value of approximately 12 m,
 580 likely due to recent surface cooling. This surface inversion, together with the slightly stable to
 581 near-neutral part of the boundary layer above, would limit recent vertical mixing of aerosols
 582 from the ground into higher layers of the troposphere. However, while surface mixing layer
 583 height reflects momentary conditions and can vary within minutes to hours, the aerosol and
 584 humidity profiles represent the integrated effects of mixing over longer time scales. We
 585 therefore concluded that the current coupling state is not a reliable indicator of the actual
 586 mixing state of the atmospheric boundary layer.

587 Furthermore, as noted in Section 2.1, Ny-Ålesund's complex orography can induce localized
 588 turbulent mixing even under stable stratification. During the descent, the wind speed profile
 589 clearly revealed the presence of a low-level jet, with a wind speed maximum at least 2 m s^{-1}
 590 higher than the minimum values both above and below. This low-level jet is a significant
 591 additional source of turbulence and vertical mixing within the boundary layer (Egerer et al.,
 592 2023). At the ground, N_{150} was around 60 cm^{-3} , and gradually decreased to 45 cm^{-3} at the
 593 balloon's sampling height, indicating a fairly uniform aerosol number distribution and a
 594 dominant influence of primary ground-level emissions. Combined with the nearly constant
 595 specific humidity ($\sim 0.7\text{--}0.8 \text{ g kg}^{-1}$), a slight increase of wind speed with altitude measured
 596 during the balloon's ascent, the low-level jet observed at the decent and a consistent wind
 597 direction on the measurement day (**Figure 3a**), these observations suggest that the boundary
 598 layer was largely well-mixed.

599 For this event, chemical analyses from both HALFBACs (**Figure 3a**) showed similar, sometimes
 600 almost identical, concentrations of almost all inorganic ions (sodium: $240 \text{ \& } 223 \text{ ng m}^{-3}$,
 601 chloride: $586 \text{ \& } 543 \text{ ng m}^{-3}$, sulfate: $336 \text{ \& } 330 \text{ ng m}^{-3}$, calcium: $87 \text{ \& } 92 \text{ ng m}^{-3}$, magnesium:
 602 $9.5 \text{ \& } 7.8 \text{ ng m}^{-3}$, potassium: $34 \text{ \& } 30 \text{ ng m}^{-3}$, oxalate ($34 \text{ \& } 37 \text{ ng m}^{-3}$) and major CCHO-bound



monosaccharide compounds (Glc_{CCHO} : 17 & 9.1 ng m^{-3} , Xyl_{CCHO} : 5.0 & 4.7 ng m^{-3} , Ara_{CCHO} : 1.2 & 0.9 ng m^{-3}) at the ground and at the balloon. As outlined above, there are clear indications for a well-mixed boundary layer, as evidenced by the similar concentrations of all these compounds, including marine CCHO_{aer} , at both the ground and balloon. Despite their potentially diverse origins—such as SSA, terrestrial dust, anthropogenic emissions, and secondary formation processes—the vertical distribution of aerosol particle constituents remained uniform. The major inorganic compounds sodium, chloride, and sulfate were also measured at the Zeppelin Observatory with a 24-hour time resolution, showing only slightly lower concentrations and good agreement with the chemical results from the balloon.

Back-trajectory analysis for three arrival heights—ground, balloon, and Zeppelin Observatory (**Figure 4, Case I**)—revealed that air masses at all levels followed the same path within the 48 hours before sampling. Originating from the Arctic pack ice, they crossed the marginal ice zone with a short residence time before passing over the ice-free ocean and Kongsfjorden, where most SSA compounds were likely taken up. The back-trajectory heights indicate a vertical connection between the three air masses, confirming a similar transport history, influenced by the same emission sources.

This case demonstrates that major SSA particle constituents, including Na^+_{aer} , Cl^-_{aer} , and CCHO_{aer} , can mix effectively within the boundary layer. Under favorable meteorological conditions, this mixing allows these compounds to reach elevated altitudes relevant to cloud formation, maintaining concentrations nearly identical to those at the ground. Moreover, such a mixed state can persist even during temporarily decoupled conditions, provided there is no additional aerosol particle source at the ground or aloft.

Case II: Free troposphere decoupled from the ground

On 27 September 2021, balloon measurements were conducted at a median altitude of 1112 m—significantly higher than both the Zeppelin Observatory and the balloon in Case I. At this altitude, the balloon had ascended beyond the boundary layer and into the free troposphere. This observation is supported by the strong increase of potential temperature between 700 m ($\theta \approx 274$ K) and 900 m ($\theta \approx 280$ K) in the vertical profile (**Figure 3b**), indicating a significant temperature inversion. N_{150} concentrations were highest near the ground and remained stable within the lower 200 m. Above this layer, values gradually decreased up to around 700 m. From there, they increased slightly toward 1112 m, likely indicating influence



634 from sources other than the ground. Specific humidity also showed substantial variability,
 635 fluctuating between 2.6 and 4 g kg⁻¹, further confirming the decoupled state of the sampled
 636 layer.

637 During active aerosol particle sampling at the ground, the average temperature was 3°C, with
 638 a relative humidity of 89% and a mean wind speed of 0.7 m s⁻¹, predominantly from the
 639 southwest (**Table S5**). In contrast, at balloon altitude, the air was slightly colder, with a mean
 640 temperature of -1.9°C, a relative humidity of 87%, and a significantly higher average wind
 641 speed of 5.5 m s⁻¹, primarily from the south and southwest (**Table S4**). On that day, IWP was
 642 high increasing from 13 kg m⁻² to about 15 kg m⁻² during the balloon sampling (**Figure S6b**). A
 643 dense layer of warm front clouds was present between 2 and 8 km, mainly consisting of cloud
 644 ice with IWP values up to 1.4 kg m⁻² (**Figure S6b**). No precipitation reached the balloon or the
 645 ground up to the last 15–30 minutes of sampling, when snowfall reached the balloon and
 646 sampling was stopped.

647 On this date, we observed a strong vertical gradient in both Na⁺_{aer} and CCHO_{aer} concentrations
 648 (**Figure 3b**), starting from the winch (Na⁺_{aer}: 1840 ng m⁻³, CCHO_{aer}: 199 ng m⁻³), decreasing at
 649 the Zeppelin Observatory (Na⁺_{aer}: 850 ng m⁻³), and dropping sharply at the balloon's altitude
 650 (Na⁺_{aer}: 23 ng m⁻³, CCHO_{aer}: 8.6 ng m⁻³). Similarly, decreasing trends with altitude were
 651 observed for other constituents, including sulfate (580; 220; 76 ng m⁻³), chloride (4230; 1500;
 652 60 ng m⁻³), and calcium (165; 32; 28 ng m⁻³). This pronounced decline in major inorganic ions
 653 and CCHO_{aer} concentrations with increasing altitude suggests a separation of ground-level air
 654 masses and those at higher elevations. It is unlikely that the substances detected at 1112 m
 655 originated primarily from fresh local sea spray emissions from Kongsfjorden or the west coast
 656 of Svalbard.

657 This assumption is supported by back-trajectory analysis (**Figure 4b**). While air masses arriving
 658 at 50 m and 474 m originated from the pack ice region in the central Arctic Ocean with a
 659 subsequent residence time over the ice-free Fram Strait, the air mass arriving at 1112 m
 660 followed a different pathway, passing over the Barents Sea near Franz Josef Land. 48 hours
 661 before sampling, this air mass had come into contact with the ground and the marine
 662 boundary layer in that region. However, after leaving the vicinity of Franz Josef Land, it
 663 remained predominantly at altitudes between 1000 and 1800 m. This suggests that SSA



emissions contributing to the measured concentrations at 1112 m in Ny-Ålesund likely originated from that distant region.

In summary, Case II demonstrates that in the presence of an atmospheric inversion, major SSA constituents, including sodium, calcium, chloride, sulfate and CCHO, can be present at higher altitudes. However, in contrast to the mixed boundary layer (Case I), they occur at concentrations different from those at the ground and likely originate from more distant emission sources through long-range transport.

Case III: Inside and below a drizzling cloud

On 03 October 2021, the ground temperature was 3°C with a high relative humidity of 89%. Winds were light, shifting between east, south, and west at 0.7 m s⁻¹ during sampling. At the balloon's altitude of 666 m, the average temperature was -1.3°C, the relative humidity 96% and the wind speed 6.8 m s⁻¹ from the east and northeast. The day was overcast, with continuous drizzle from a 2 km deep mixed-phase cloud layer with LWP values of up to 300 g m⁻² and I WV of around 13 to 14 kg m⁻². The balloon's altitude was close to the melting layer.

During the balloon's ascent and descent to the aerosol sampling height of 666 m, a positive gradient in potential temperature was observed (272 K at the ground vs. 278 K at the balloon, **Figure 3c**) indicating a stably stratified boundary layer. Similar to Case I, the specific humidity remained relatively uniform throughout the vertical column, with values between 3.2 and 3.8 g kg⁻¹. The vertical N₁₅₀ distribution showed generally lower aerosol number concentrations compared to Case I, ranging between 3 and 10 cm⁻³, and exhibited greater relative fluctuation. In summary, the boundary layer mixing conditions on 03 October 2021 (Case III) appeared similar to those in Case I. The key difference, however, was that in this case, aerosol sampling occurred partially inside or below a drizzling low-level cloud.

Back-trajectory analysis for ground, balloon, and Zeppelin Observatory (**Figure 4, Case III**) showed that air masses at all arrival heights followed the same path within the 48 hours before sampling, originating from the ice-free ocean south of Svalbard. As observed in Case I, trajectory heights indicate a vertical movement during this period, suggesting that air masses at all three levels shared a similar transport history and were influenced by the same emission sources.



694 In line with the lower aerosol number concentrations, offline measurements of chemical
 695 constituents were also generally lower than in the previous cases. Furthermore, major
 696 inorganic ions (**Figure 3c**) were similar or slightly higher at the ground than at the balloon
 697 (chloride: 289 & 252 ng m⁻³; sulfate: 66 & 59 ng m⁻³; Na⁺: 53 & 35 ng m⁻³; K⁺: 23 & 20 ng m⁻³).
 698 At the Zeppelin Observatory, only Na⁺ was measured above the detection limit, which was
 699 quantified at 38 ng m⁻³—almost identical to the concentration measured at the balloon. This
 700 consistency indicates a rather mixed boundary layer. Creamean et al. (2021) analyzed three
 701 years of Arctic aerosol vertical distributions using a tethered balloon in Alaska and found that,
 702 when a uniform aerosol distribution below clouds was observed, it primarily occurred in
 703 autumn, aligning well with Case III.

704 Interestingly, despite the same levels of major inorganic ions, some chemical constituents
 705 exhibited increased concentrations at higher altitudes. These included major
 706 monosaccharides bound within CCHO (ground & balloon: Glc_{CCHO}: 12.6 & 34 ng m⁻³; Xyl_{CCHO}:
 707 0.57 & 4.4 ng m⁻³; Ara_{CCHO}: below detection limit & 0.97 ng m⁻³), as well as oxalate (5.5 &
 708 24 ng m⁻³), Ca²⁺ (47 & 187 ng m⁻³), and Mg²⁺ (0.97 & 2.6 ng m⁻³). The origin of these elevated
 709 concentrations remains unclear, as neither local sea spray emissions nor remote sources
 710 appeared suitable to account for the observed patterns.

711 While organics like CCHO_{aer} and oxalate_{aer} might originate through secondary in-situ
 712 atmospheric chemical or microbial processes—particularly in the aqueous phase, as discussed
 713 more in detail in the following section—this does not apply for inorganic elements such as
 714 calcium and magnesium. Instead, their ionic forms were possibly released from preexisting
 715 complex organic structures in SSA particles, becoming soluble and thus detectable by our
 716 analytical methods. OM-bound Ca²⁺, as already found in Antarctic SSA (Su et al., 2023), may
 717 originate from SML-derived polysaccharide gels and airborne algal cells or fragments, which
 718 can release Ca²⁺ and Mg²⁺ through gel dispersion or cell dissolution under the acidic conditions
 719 of chemically aged SSA aerosol particles (Aller et al., 2017; Angle et al., 2021; Orellana and
 720 Leck, 2015; van Pinxteren et al., 2022; Trainic et al., 2018; Zhu et al., 2014).

721 In summary, Case III, demonstrates that certain organic SSA constituents can change within
 722 the vertical column due to atmospheric aging after primary emissions and vertical transport.

723



724 Overall, the three cases presented highlight distinct meteorological scenarios that can lead to
725 similar, lower, or even higher concentrations of chemical constituents at different altitudes.
726 Interestingly, comparable patterns, with higher, lower, or similar levels at ground and balloon
727 altitude, were also observed at the North Pole by Porter et al. (2022), who measured INP
728 concentrations and combined these with trajectory analyses and heat sensitivity tests to
729 conclude on their sources. While this effect-based approach provides valuable insights into
730 aerosol particle properties, direct chemical analyses, as performed in this study, can further
731 enhance certainty regarding the origin and composition of particles relevant for cloud droplet
732 and cloud ice formation.



3.3 Factors affecting SSA constituents beyond local sea-air transfer

Long-range transport and size-dependent deposition

SSA particles originate from both local and remote marine regions. However, our sampling methods make it challenging to determine the relative contribution of long-range transported SSA constituents, particularly when a local marine source, such as the Kongsfjorden is adjacent to the sampling site and may dominate other marine emissions.

As demonstrated in Case II, long-range transport of SSA can become dominant when air masses at elevated altitudes are decoupled from those at the ground. In this case, vertical and horizontal trajectory analysis suggests that the measured SSA constituents may have been emitted and incorporated into the atmosphere approximately 48 hours earlier over the Barents Sea, near Franz Josef Land. Atmospheric processes, such as the removal of larger supermicron particles, cloud activation, and precipitation, likely reduced their absolute mass concentration by one to two orders of magnitude before the arrival of the air masses in Ny-Ålesund.

In several balloon-borne TSP filter samples, however, an elevated CCHO/Na⁺ ratio was observed, most notably on 24 September 2021; 03 October 2021 (Case III); 03 April 2022 (see **Figure 2d**). These values far exceeded both ground-based aerosol measurements from this study and previously reported values (Zeppenfeld et al., 2021, 2023), particularly for supermicron SSA particles that dominate the TSP mass. A slight increase of this ratio may be explained by a longer atmospheric residence time of these particles, leading to a relative reduction of supermicron aerosol particles through deposition (Croft et al., 2009; Hoppel et al., 2002), which are typically dominated by sea salt (O'Dowd and de Leeuw, 2007), while submicron aerosol particles—rich in surface-active CCHO—remain. This could lead to a shift of the CCHO/Na⁺ ratios more similar to submicron than supermicron particles in the TSP samples of this study, as seen in Case II.

However, in the three cases with the most pronounced increase of the CCHO_{aer}/Na⁺_{aer} ratios in TSP at higher altitudes (24 September 2021; 03 October 2021; 03 April 2022), absolute CCHO_{aer} concentrations were elevated as well (compare **Figures 2b and 2d**). Such increases of absolute concentrations cannot be explained by selective removal processes. This raises the question of whether the observed CCHO_{aer} concentrations could result from the long-range



763 transport of SSA compounds from a distant marine source with significantly higher CCHO
 764 levels in the seawater than the local Kongsfjorden.

765 Model simulations using FESOM2.1-REcoM3 (Gürses et al., 2023) (**Figure S7**) and field data
 766 (Assmy et al., 2023; Feltracco et al., 2021; Grosse et al., 2021; Wietz et al., 2024) confirm that
 767 the eastern Fram Strait as well as coastal Svalbard waters are productive and polysaccharide-
 768 rich regions. While the FESOM2.1-REcoM3 model does not resolve the SML separately,
 769 previous studies have shown significant CCHO enrichment in this layer (Compiano et al., 1993;
 770 Engel and Galgani, 2016; Gao et al., 2012; Zäncker et al., 2021), particularly in the productive
 771 marginal ice zone (Zeppenfeld et al., 2023). However, in the cases of high CCHO_{aer} at elevated
 772 altitudes in the current study, air mass trajectories did not cross the marginal ice zone within
 773 48 hours before reaching Svalbard (**Figure S8**). These findings suggest that long-range
 774 transport of SSA from more productive marine sources is unlikely to explain elevated CCHO_{aer}
 775 concentrations at elevated altitudes within the lower troposphere, further supporting a rather
 776 local source or atmospheric in-situ formation.

777 In summary, while long-range transport of SSA constituents at elevated altitudes appears
 778 relevant in cases of decoupled atmospheric layers such as in Case II, it may not explain the
 779 significantly higher CCHO_{aer} concentrations at high altitudes compared to ground levels.
 780 Instead, in-situ formation of CCHO_{aer} could be a more plausible explanation for these
 781 observations.

782

783 ***Atmospheric in-situ formation of marine CCHO_{aer}***

784 Bacteria can be transported into and persist in the Arctic atmosphere (Jensen et al., 2022;
 785 Šantl-Temkiv et al., 2018), with sources including terrestrial environments and surface
 786 seawater, particularly the SML (Aller et al., 2005). Our field study confirmed such dynamics by
 787 finding diverse marine and terrestrial bacteria in aerosol particles collected at the Old Pier
 788 (Wietz et al., to be submitted). Some aerosolized taxa, for instance *Polaribacter*, encode
 789 multiple genes for CCHO metabolism (Avci et al., 2020) and consistently occur in the
 790 Kongsfjorden atmosphere during the spring bloom (Feltracco et al., 2021). These observations
 791 might underpin microbial CCHO transformations in the atmosphere, for instance the
 792 production of sticky, polysaccharide-based gels as protection against temperature
 793 fluctuations, salinity changes, and desiccation (Aller et al., 2005; Ramasamy et al., 2023; Šantl-



794 Temkiv et al., 2022). Under highly humid conditions—especially in the presence of liquid water
 795 (such as in Case III)—airborne bacteria can become metabolically active (Ervens and Amato,
 796 2020; Haddrell and Thomas, 2017). Atmospheric OM formation, including CCHO, through
 797 microbial activity has been documented for cloud water and aerosol particles (Bianco et al.,
 798 2019; Klein et al., 2016; Matulová et al., 2014). Consequently, metabolically active bacteria in
 799 the atmosphere could explain the increased CCHO_{aer} concentrations observed within or near
 800 drizzling clouds in Case III of this study.

801 ***CCHO_{aer} versus oxalate_{aer}: Co-production or atmospheric processing?***

802 Since both combined glucose and combined xylose were consistently detected in CCHO_{aer} of
 803 nearly all aerosol samples, we examined their correlation with other atmospheric chemical
 804 parameters. We observed a strong correlation between atmospheric xylose in CCHO_{aer} and
 805 oxalate_{aer} with an $R=0.78$ ($p<0.001$) across all sampling locations and heights (**Figure 5**).
 806 Oxalate, the ionic form of oxalic acid, is the most abundant dicarboxylic acid in aerosol
 807 particles (Kerminen et al., 1999; Rinaldi et al., 2011), with atmospheric concentrations in this
 808 study between <1 and 67 ng m^{-3} . The strong correlation raised the question of whether oxalic
 809 acid could be chemically linked to combined carbohydrates in aerosol particles.

810 Oxalate_{aer} is known to originate from several primary sources and secondary formation
 811 pathways in both terrestrial and anthropogenic environments (Kawamura and Bikkina, 2016;
 812 Yang et al., 2022). In remote marine environments, the atmospheric formation of oxalic acid
 813 was proposed by Warneck (2003) through the aqueous-phase oxidation of glyoxal and
 814 glycolaldehyde, a process also investigated by field measurements inside and above marine
 815 clouds (Crahan et al., 2004; Sorooshian et al., 2007) and modeling (Herrmann et al., 2005;
 816 Tilgner and Herrmann, 2010). The possible aqueous-phase formation was supported by Case
 817 III of this study, where higher oxalate_{aer} concentrations were observed within and in vicinity of
 818 clouds compared to ground level. In contrast, in the drier conditions of Cases I and II, oxalate_{aer}
 819 levels remained vertically uniform. Additionally, since overall oxalate_{aer} levels at the Old Pier
 820 ($1.1\text{--}10.1 \text{ ng m}^{-3}$; $\text{mean}=4.3\pm3.5 \text{ ng m}^{-3}$) were relatively low compared to the more inland
 821 Winch ($<1\text{--}58 \text{ ng m}^{-3}$; $\text{mean}=19.8\pm16.2 \text{ ng m}^{-3}$) and elevated altitudes samples ($4.6\text{--}67 \text{ ng m}^{-3}$;
 822 $\text{mean}=29.6\pm17.8 \text{ ng m}^{-3}$), direct primary oceanic emission was likely not its dominant source.



823

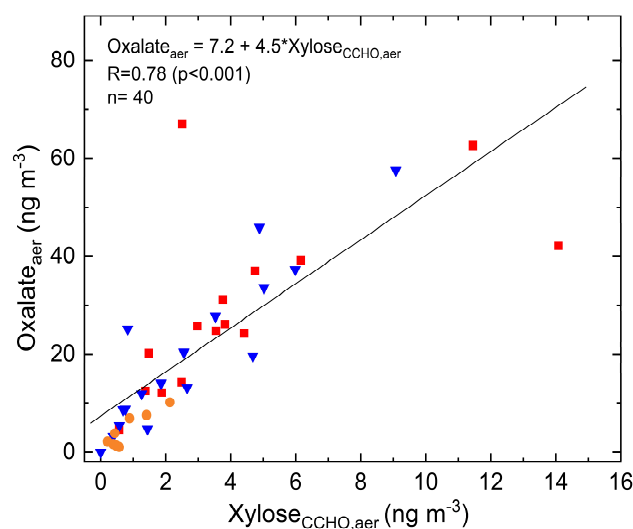


Figure 5. Atmospheric oxalate as a function of xylose in CCHO_{aer} ($R=0.78$; $p<0.001$) measured in TSP from the Old Pier (orange circles), the winch site (blue triangles) and at elevated altitudes (red squares).

832 But what are the precursors of oxalic acid's precursors? While Warneck (2003) suggested that
 833 the anthropogenic volatile organic compounds acetylene and ethene can be transformed to
 834 atmospheric glyoxal, other studies suggest the photochemical degradation of marine OM
 835 (McNeill, 2015; Sinreich et al., 2010; Turekian et al., 2003; Zhou et al., 2014), with oligo- and
 836 polysaccharides representing a known subclass. Although not explicitly measured in this
 837 study, previous findings have shown that both CCHO_{aer} (Leck et al., 2013; Zeppenfeld et al.,
 838 2021, 2023) and oxalate_{aer} (Guo et al., 2016; Rinaldi et al., 2011; Turekian et al., 2003) are
 839 present across both the accumulation and coarse size modes. However, no consistently
 840 dominant size mode has been identified, which may support a common mechanism of
 841 formation or similar atmospheric processing pathways.

842 Here, based on known chemical reactions, we propose possible atmospheric pathways linking
 843 xylose-containing oligo- and polysaccharides as the precursors to oxalate as the final product
 844 (**Figure 6**). The initial depolymerization of CCHO presumably occurs either via enzymatic
 845 degradation, e.g. by glycoside hydrolases, or acid hydrolysis (Panagiotopoulos and Sempéré,
 846 2005), both of which are plausible in the atmospheric context. Active microbial enzymes have
 847 been detected in SSA, often exhibiting activities 1–2 orders of magnitude higher than in bulk
 848 seawater (Malfatti et al., 2019). Additionally, SSA particles are known for reaching very low pH



849 levels within minutes after their emissions due to the uptake and reactions with acidic gases,
 850 as well as water loss (Angle et al., 2022, 2021). Furthermore, although not explicitly
 851 investigated in an atmospheric context, Zhu et al. (2023) observed rapid depolymerization of
 852 xylose-containing oligosaccharides into the monosaccharide xylose within minutes in a
 853 UV/H₂O₂ system, generating hydroxyl radicals.

854

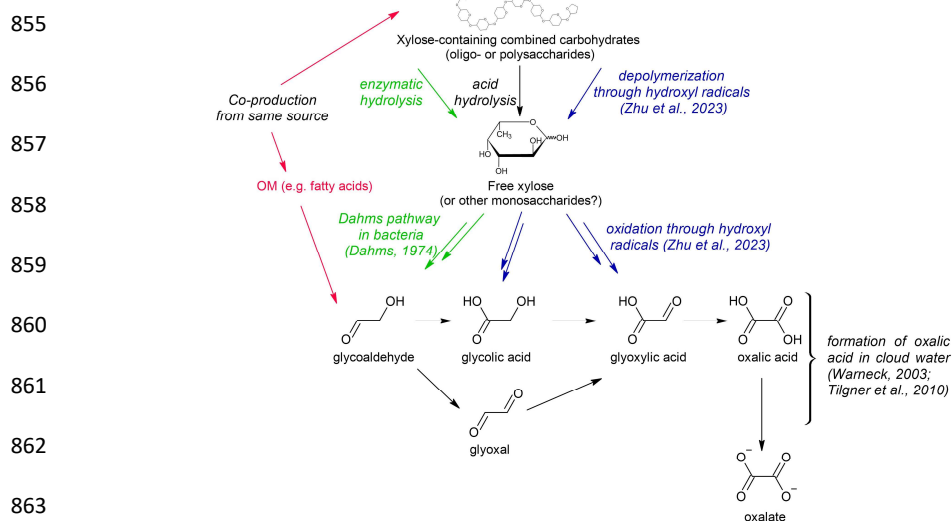


Figure 6. Possible pathways for the formation of atmospheric oxalate from xylose in combined carbohydrates in marine aerosol particles.

864 Free xylose was—with one exception—never detected in any aerosol sample of this study,
 865 suggesting that it is rapidly processed in the atmosphere. Two potential pathways may link
 866 monomeric xylose to precursors of Warneck’s oxalate formation: (1) a follow-up reaction with
 867 hydroxyl radicals, where the pyranose ring of xylose is cleaved after the more susceptible
 868 glycosidic bonds have been readily broken. Zhu et al. (2023) observed glycolic acid and
 869 glyoxylic acid among other products following the UV/H₂O₂ treatment of xylooligosaccharides.
 870 (2) Bacterial metabolism via the Dahms pathway converting free xylose into pyruvate and
 871 glycolaldehyde (Dahms, 1974). However, only few bacteria encode this pathway; and it is
 872 highly questionable whether these occur in sufficient atmospheric concentrations for a
 873 measurable effect.



874 One indication that direct formation from xylose-containing oligo- and polysaccharides cannot
875 be the sole source of atmospheric oxalate in the marine environment is the discrepancy in
876 concentrations: atmospheric oxalate levels were seven times higher than those of combined
877 xylose. This confirms the involvement of additional precursors or a co-production/co-emission
878 of combined xylose with gaseous precursors, such as isoprene (Carlton et al., 2009; Kawamura
879 and Bikkina, 2016), or other primary marine organic matter, such as phytoplankton-derived
880 fatty acids (Kawamura et al., 1996b, a) undergoing photo-oxidation. Further targeted
881 laboratory and modeling studies are needed for clarity.



4. Summary and Atmospheric Implications

In autumn 2021 and spring 2022, we performed balloon-borne measurements of major SSA constituents at Ny-Ålesund (Svalbard). Our evidence demonstrated that both sodium and marine CCHO reach elevated altitudes within the boundary layer, and even the free troposphere as part of aerosol particles. The relationship between ground-level and high-altitude measurements was strongly influenced by meteorological conditions and the mixing state of the lower atmosphere, as discussed in three representative cases. Long-range transport of Na^+_{aer} and CCHO_{aer} from remote marine sources is presumably relevant for high-altitude measurements, especially when the upper air masses were decoupled from the ground. However, in cases of a well-mixed lower atmosphere, the local marine source (here, the Kongsfjorden) was the dominant contributor for atmospheric Na^+_{aer} and CCHO_{aer} . Under very humid conditions particularly in the presence of liquid precipitating clouds, in-situ formation of CCHO_{aer} was observed, possibly linked to microbial metabolism. To establish more generalizable patterns, we recommend further field studies using airborne platforms.

The significant correlation between combined xylose within CCHO_{aer} , and oxalate_{aer} suggests underlying pathways for oxalic acid formation from combined xylose and other monosaccharide units within CCHO_{aer} ; alternatively, a co-production of xylose-containing oligo- and polysaccharides alongside oxalate precursors.

CCNs and INPs are key drivers in cloud formation, influencing radiative and precipitation properties and, consequently, climate processes. Considerable uncertainties remain regarding the origin and chemical composition of these particles, particularly in remote Arctic regions, which affects the accuracy of climate models. Since marine polysaccharides have been identified as relevant ice-nucleating molecules in the remote marine atmosphere (Hartmann et al., 2025), our findings have implications for cloud microphysics, especially given that these carbohydrates are transported to altitudes relevant for cloud formation. Furthermore, atmospheric processing, as observed here, may alter the ice-nucleating properties of these macromolecules, potentially creating new INPs in-situ or deactivating existing ones.

As the Arctic continues to change, expanding ice-free ocean areas will serve as emission sources for SSA particles, influencing cloud properties, and finally the radiative budget.



911 Consequently, our findings contribute to an improved understanding of the complex interplay
912 of environmental processes resulting in Arctic amplification (Wendisch et al., 2017, 2023).

913 **Author contributions**

914 SZ wrote the manuscript with input from all co-authors. SZ, JS, CP, HS, BW, MW, and MvP
915 collected field samples in Ny-Ålesund. HS and BW served as principal investigators for balloon
916 operations during the field campaign. SZ conducted the laboratory carbohydrate analyses and
917 data processing. MZ and AB carried out the FESOM2.1-REcoM3 simulations. KE assessed cloud
918 conditions for the case studies using remote sensing data. All co-authors reviewed and
919 commented on the manuscript.

920

921 **Acknowledgments**

922 We would like to express our gratitude to Kings Bay and the AWIPEV staff, with special thanks
923 to the station leader Grégory Tran, for their invaluable support to make this field study
924 possible. We furthermore thank the AWIPEV station's scientific staff in ensuring the
925 availability of high-quality meteorological data. In this context, we like to give special thanks
926 to Fieke Rader and Marion Maturilli. The cloud observations were taken within the project
927 AWIPEV_0016.

928 We also thank the scientific team at the Zeppelin Observatory from NILU and NPI, with special
929 appreciation to Wenche Aas, for their dedicated work in monitoring aerosol data.

930 Furthermore, we acknowledge the entire BELUGA team for their contributions during both
931 the autumn 2021 and spring 2022 campaigns, with special thanks to Thomas Conrath. We also
932 thank Michel Michalkow for preprocessing the CAMP and standard meteorological data
933 collected at BELUGA as part of his Master's thesis. We are grateful to René Rabe for preparing
934 the campaign equipment and to Leon Schmidt for conducting the chemical analysis of
935 inorganic ions.

936 For the FESOM2.1-REcoM3 simulation for this research, the authors gratefully acknowledge
937 the computing time granted by the Resource Allocation Board and provided on the
938 supercomputer Lise and Emmy at NHR@ZIB and NHR@Göttingen as part of the NHR



939 infrastructure. The calculations for this research were conducted with computing resources
940 under the project hbk00084.

941 This research has been supported by the Deutsche Forschungsgemeinschaft (DFG, German
942 Research Foundation, project no. 268020496-TRR 172) within the Transregional Collaborative
943 Research Center “Arctic Amplification: Climate Relevant Atmospheric and SurfaCe Processes,
944 and Feedback Mechanisms (AC)3” in subprojects A02, B04, C03 and E02. We thank Johannes
945 Röttenbacher for his constructive feedback on the manuscript.

946

947 **Competing interests**

948 All authors declare no financial or non-financial competing interests. Some authors are
949 members of the editorial board of ACP.

950

951 **Data availability**

952 Chemical data from offline TSP filters are publicly available in PANGAEA for seawater
953 (Zeppenfeld and Schmidt, 2025) and aerosol particles (Zeppenfeld et al., 2025). The
954 microwave radiometer LWP and IWV data are available in PANGAEA (Ebell and Ritter, 2022).
955 The Cloudnet classification and ice water content products (Ebell et al., 2025) can be
956 downloaded via the ACTRIS Cloudnet data portal (<https://cloudnet.fmi.fi>).



957 References

- 958 Aas, W., Berglen, T. F., Eckhardt, S., Fiebig, M., Solberg, S., and Yttri, K. E.: Monitoring of long-range transported air pollutants
 959 in Norway. Annual Report 2021., NILU, 2022.
- 960 Aas, W., Eckhardt, S., Solberg, S., and Yttri, K. E.: Monitoring of long-range transported air pollutants in Norway. Annual Report
 961 2022., NILU, 2023.
- 962 Akansu, E. F., Dahlke, S., Siebert, H., and Wendisch, M.: Evaluation of methods to determine the surface mixing layer height
 963 of the atmospheric boundary layer in the central Arctic during polar night and transition to polar day in cloudless and cloudy
 964 conditions, *Atmospheric Chemistry and Physics*, 23, 15473–15489, <https://doi.org/10.5194/acp-23-15473-2023>, 2023.
- 965 Aller, J. Y., Kuznetsova, M. R., Jahns, C. J., and Kemp, P. F.: The sea surface microlayer as a source of viral and bacterial
 966 enrichment in marine aerosols, *Journal of Aerosol Science*, 36, 801–812, <https://doi.org/10.1016/j.jaerosci.2004.10.012>,
 967 2005.
- 968 Aller, J. Y., Radway, J. C., Kilhau, W. P., Bothe, D. W., Wilson, T. W., Vaillancourt, R. D., Quinn, P. K., Coffman, D. J., Murray,
 969 B. J., and Knopf, D. A.: Size-resolved characterization of the polysaccharidic and proteinaceous components of sea spray
 970 aerosol, *Atmospheric Environment*, 154, 331–347, <https://doi.org/10.1016/j.atmosenv.2017.01.053>, 2017.
- 971 Alpert, P. A., Kilhau, W. P., O'Brien, R. E., Moffet, R. C., Gilles, M. K., Wang, B., Laskin, A., Aller, J. Y., and Knopf, D. A.: Ice-
 972 nucleating agents in sea spray aerosol identified and quantified with a holistic multimodal freezing model, *Science Advances*,
 973 8, eabq6842, <https://doi.org/10.1126/sciadv.abq6842>, 2022.
- 974 Aluwihare, L. I., Repeta, D. J., and Chen, R. F.: A major biopolymeric component to dissolved organic carbon in surface sea
 975 water, *Nature*, 387, 166–169, <https://doi.org/10.1038/387166a0>, 1997.
- 976 Amore, A., Giardi, F., Becagli, S., Caiazzo, L., Mazzola, M., Severi, M., and Traversi, R.: Source apportionment of sulphate in
 977 the High Arctic by a 10 yr-long record from Gruvebadet Observatory (Ny-Ålesund, Svalbard Islands), *Atmospheric*
 978 *Environment*, 270, 118890, <https://doi.org/10.1016/j.atmosenv.2021.118890>, 2022.
- 979 Angle, K., Grassian, V. H., and Ault, A. P.: The rapid acidification of sea spray aerosols, *Physics today*, 75, 58–59,
 980 <https://doi.org/10.1063/PT.3.4926>, 2022.
- 981 Angle, K. J., Crocker, D. R., Simpson, R. M. C., Mayer, K. J., Garofalo, L. A., Moore, A. N., Garcia, S. L. M., Or, V. W., Srinivasan,
 982 S., Farhan, M., Sauer, J. S., Lee, C., Pothier, M. A., Farmer, D. K., Martz, T. R., Bertram, T. H., Cappa, C. D., Prather, K. A., and
 983 Grassian, V. H.: Acidity across the interface from the ocean surface to sea spray aerosol, *PNAS*, 118, 1–6,
 984 <https://doi.org/10.1073/pnas.2018397118>, 2021.
- 985 Arnosti, C., Wietz, M., Brinkhoff, T., Hehemann, J.-H., Probandt, D., Zeugner, L., and Amann, R.: The Biogeochemistry of
 986 Marine Polysaccharides: Sources, Inventories, and Bacterial Drivers of the Carbohydrate Cycle, *Ann Rev Mar Sci*, 13, 81–108,
 987 <https://doi.org/10.1146/annurev-marine-032020-012810>, 2021.
- 988 Assmy, P., Cecilie Kvernvik, A., Hop, H., Hoppe, C. J. M., Chierici, M., David T., D., Duarte, P., Fransson, A., García, L. M., Patuła,
 989 W., Kwaśniewski, S., Maturilli, M., Pavlova, O., Taterek, A., Wiktor, J. M., Wold, A., Wolf, K. K. E., and Bailey, A.: Seasonal
 990 plankton dynamics in Kongsfjorden during two years of contrasting environmental conditions, *Progress in Oceanography*,
 991 213, 102996, <https://doi.org/10.1016/j.pocean.2023.102996>, 2023.
- 992 Avci, B., Krüger, K., Fuchs, B. M., Teeling, H., and Amann, R. I.: Polysaccharide niche partitioning of distinct *Polaribacter* clades
 993 during North Sea spring algal blooms, *ISME J*, 14, 1369–1383, <https://doi.org/10.1038/s41396-020-0601-y>, 2020.
- 994 Barthelmeß, T., Cristi, A., Deppeler, S., Safi, K., Sellegri, K., Law, C. S., and Engel, A.: Pronounced Diel Cycling of Dissolved
 995 Carbohydrates and Amino Acids in the Surface Ocean and across Diverse Regimes, *Environ. Sci. Technol.*, 59, 419–429,
 996 <https://doi.org/10.1021/acs.est.4c00491>, 2025.
- 997 Becker, S., Tebben, J., Coffinet, S., Wiltshire, K., Iversen, M. H., Harder, T., Hinrichs, K.-U., and Hehemann, J.-H.: Laminarin is
 998 a major molecule in the marine carbon cycle, *PNAS*, 117, 6599–6607, <https://doi.org/10.1073/pnas.1917001117>, 2020.
- 999 Bianco, A., Deguillaume, L., Chaumerliac, N., Vařtilingom, M., Wang, M., Delort, A.-M., and Bridoux, M. C.: Effect of
 1000 endogenous microbiota on the molecular composition of cloud water: a study by Fourier-transform ion cyclotron resonance
 1001 mass spectrometry (FT-ICR MS), *Sci Rep*, 9, 1–12, <https://doi.org/10.1038/s41598-019-44149-8>, 2019.
- 1002 Bischof, K., Convey, P., Duarte, P., Gattuso, J.-P., Granberg, M., Hop, H., Hoppe, C., Jiménez, C., Lisitsyn, L., Martínez, B.,
 1003 Roleda, M. Y., Thor, P., Wiktor, J. M., and Gabrielsen, G. W.: Kongsfjorden as Harbinger of the Future Arctic: Knowns,
 1004 Unknowns and Research Priorities, in: *The Ecosystem of Kongsfjorden, Svalbard*, edited by: Hop, H. and Wiencke, C., Springer
 1005 International Publishing, Cham, 537–562, https://doi.org/10.1007/978-3-319-46425-1_14, 2019.
- 1006 Bivand, R., Pebesma, E., and Gomez-Rubio, V.: *Applied spatial data analysis with R*, Springer, 2013.
- 1007 Bivand, R., Keitt, T., and Rowlingson, B.: *rgdal: Bindings for the “Geospatial” Data Abstraction Library*, R package version 1.5-
 1008 32, 2022.



- 1009 Borch, N. H. and Kirchman, D. L.: Concentration and composition of dissolved combined neutral sugars (polysaccharides) in
1010 seawater determined by HPLC-PAD, *Marine Chemistry*, 57, 85–95, [https://doi.org/10.1016/S0304-4203\(97\)00002-9](https://doi.org/10.1016/S0304-4203(97)00002-9), 1997.
- 1011 Brownrigg, M. R.: Package ‘mapdata’, R package version 2.3.1, 2013.
- 1012 Brownrigg, M. R.: maps: Draw Geographical Maps, R package version 3.4.2, 2023.
- 1013 Browse, J., Carslaw, K. S., Mann, G. W., Birch, C. E., Arnold, S. R., and Leck, C.: The complex response of Arctic aerosol to sea-
1014 ice retreat, *Atmospheric Chemistry and Physics*, 14, 7543–7557, <https://doi.org/10.5194/acp-14-7543-2014>, 2014.
- 1015 Burns, W. G., Marchetti, A., and Ziervogel, K.: Enhanced formation of transparent exopolymer particles (TEP) under
1016 turbulence during phytoplankton growth, *J Plankton Res*, 41, 349–361, <https://doi.org/10.1093/plankt/fbz018>, 2019.
- 1017 Burrows, S. M., Ogunro, O., Frossard, A., Russell, L. M., Rasch, P. J., and Elliott, S.: A Physically Based Framework for Modelling
1018 the Organic Fractionation of Sea Spray Aerosol from Bubble Film Langmuir Equilibria, *Atmospheric Chemistry and Physics*,
1019 14(24):13601–13629, <https://doi.org/10.5194/acp-14-13601-2014>, 2014.
- 1020 Cai, Q., Wang, J., Beletsky, D., Overland, J., Ikeda, M., and Wan, L.: Accelerated decline of summer Arctic sea ice during 1850–
1021 2017 and the amplified Arctic warming during the recent decades, *Environ. Res. Lett.*, 16, 034015,
1022 <https://doi.org/10.1088/1748-9326/abdb5f>, 2021.
- 1023 Carlton, A. G., Wiedinmyer, C., and Kroll, J. H.: A review of Secondary Organic Aerosol (SOA) formation from isoprene,
1024 *Atmospheric Chemistry and Physics*, 9, 4987–5005, <https://doi.org/10.5194/acp-9-4987-2009>, 2009.
- 1025 Carslaw, D. C. and Ropkins, K.: openair --- An R package for air quality data analysis, *Environmental Modelling & Software*,
1026 27–28, 52–61, 2012.
- 1027 Chang, L., Song, S., Feng, G., Zhang, Y., and Gao, G.: Assessment of the Uncertainties in Arctic Low-Level Temperature
1028 Inversion Characteristics in Radio Occultation Observations, *IEEE Transactions on Geoscience and Remote Sensing*, 55, 1793–
1029 1803, <https://doi.org/10.1109/TGRS.2016.2633461>, 2017.
- 1030 Chi, J. W., Li, W. J., Zhang, D. Z., Zhang, J. C., Lin, Y. T., Shen, X. J., Sun, J. Y., Chen, J. M., Zhang, X. Y., Zhang, Y. M., and Wang,
1031 W. X.: Sea salt aerosols as a reactive surface for inorganic and organic acidic gases in the Arctic troposphere, *Atmospheric
1032 Chemistry and Physics*, 15, 11341–11353, <https://doi.org/10.5194/acp-15-11341-2015>, 2015.
- 1033 Compiano, A.-M., Romano, J.-C., Garabetian, F., Laborde, P., and de la Giraudièrea, I.: Monosaccharide composition of
1034 particulate hydrolysable sugar fraction in surface microlayers from brackish and marine waters, *Marine Chemistry*, 42, 237–
1035 251, [https://doi.org/10.1016/0304-4203\(93\)90015-G](https://doi.org/10.1016/0304-4203(93)90015-G), 1993.
- 1036 Crahan, K. K., Hegg, D., Covert, D. S., and Jonsson, H.: An exploration of aqueous oxalic acid production in the coastal marine
1037 atmosphere, *Atmospheric Environment*, 38, 3757–3764, <https://doi.org/10.1016/j.atmosenv.2004.04.009>, 2004.
- 1038 Creamean, J. M., de Boer, G., Telg, H., Mei, F., Dexheimer, D., Shupe, M. D., Solomon, A., and McComiskey, A.: Assessing the
1039 vertical structure of Arctic aerosols using balloon-borne measurements, *Atmospheric Chemistry and Physics*, 21, 1737–1757,
1040 <https://doi.org/10.5194/acp-21-1737-2021>, 2021.
- 1041 Croft, B., Lohmann, U., Martin, R. V., Stier, P., Wurzler, S., Feichter, J., Posselt, R., and Ferrachat, S.: Aerosol size-dependent
1042 below-cloud scavenging by rain and snow in the ECHAM5-HAM, *Atmospheric Chemistry and Physics*, 9, 4653–4675,
1043 <https://doi.org/10.5194/acp-9-4653-2009>, 2009.
- 1044 Cunliffe, M. and Wurl, O.: Guide to best practices to study the ocean’s surface., *Marine Biological Association of the United
1045 Kingdom for SCOR*, 2014.
- 1046 Dahms, A. S.: 3-Deoxy-D-pentulosonic acid aldolase and its role in a new pathway of D-xylose degradation, *Biochemical and
1047 Biophysical Research Communications*, 60, 1433–1439, [https://doi.org/10.1016/0006-291X\(74\)90358-1](https://doi.org/10.1016/0006-291X(74)90358-1), 1974.
- 1048 Dekhtyareva, A., Holmén, K., Maturilli, M., Hermansen, O., and Graversen, R.: Effect of seasonal mesoscale and microscale
1049 meteorological conditions in Ny-Ålesund on results of monitoring of long-range transported pollution, *Polar Research*, 2018.
- 1050 DeMott, P. J., Hill, T. C. J., McCluskey, C. S., Prather, K. A., Collins, D. B., Sullivan, R. C., Ruppel, M. J., Mason, R. H., Irish, V. E.,
1051 Lee, T., Hwang, C. Y., Rhee, T. S., Snider, J. R., McMeeking, G. R., Dhaniyala, S., Lewis, E. R., Wentzell, J. J. B., Abbott, J., Lee,
1052 C., Sultana, C. M., Ault, A. P., Axson, J. L., Martinez, M. D., Venero, I., Santos-Figueroa, G., Stokes, M. D., Deane, G. B., Mayol-
1053 Bracero, O. L., Grassian, V. H., Bertram, T. H., Bertram, A. K., Moffett, B. F., and Franc, G. D.: Sea spray aerosol as a unique
1054 source of ice nucleating particles, *PNAS*, 113, 5797–5803, <https://doi.org/10.1073/pnas.1514034112>, 2016.
- 1055 Dusek, U., Frank, G. P., Hildebrandt, L., Curtius, J., Schneider, J., Walter, S., Chand, D., Drewnick, F., Hings, S., Jung, D.,
1056 Borrmann, S., and Andreae, M. O.: Size Matters More Than Chemistry for Cloud-Nucleating Ability of Aerosol Particles,
1057 *Science*, 312, 1375–1378, <https://doi.org/10.1126/science.1125261>, 2006.
- 1058 Ebell, K. and Ritter, C.: HATPRO microwave radiometer measurements at AWIPEV, Ny-Ålesund (2019–2021), *PANGAEA*,
1059 <https://doi.org/10.1594/PANGAEA.943004>, 2022.
- 1060 Ebell, K., Maturilli, M., Ritter, C., and O’Connor, E.: Custom collection of classification, and ice water content data from Ny-
1061 Ålesund between 27 Sep and 12 Nov 2021, ACTRIS Cloud remote sensing data centre unit (CLU),
1062 <https://doi.org/10.60656/5598100185854c01>, 2025.



- 1063 Egerer, U., Ehrlich, A., Gottschalk, M., Griesche, H., Neggers, R. A. J., Siebert, H., and Wendisch, M.: Case study of a humidity
1064 layer above Arctic stratocumulus and potential turbulent coupling with the cloud top, *Atmospheric Chemistry and Physics*,
1065 21, 6347–6364, <https://doi.org/10.5194/acp-21-6347-2021>, 2021.
- 1066 Egerer, U., Siebert, H., Hellmuth, O., and Sørensen, L. L.: The role of a low-level jet for stirring the stable atmospheric surface
1067 layer in the Arctic, *Atmospheric Chemistry and Physics*, 23, 15365–15373, <https://doi.org/10.5194/acp-23-15365-2023>, 2023.
- 1068 Engel, A.: Distribution of transparent exopolymer particles (TEP) in the northeast Atlantic Ocean and their potential
1069 significance for aggregation processes, *Deep Sea Research Part I: Oceanographic Research Papers*, 51, 83–92,
1070 <https://doi.org/10.1016/j.dsr.2003.09.001>, 2004.
- 1071 Engel, A. and Galgani, L.: The organic sea-surface microlayer in the upwelling region off the coast of Peru and potential
1072 implications for air–sea exchange processes, *Biogeosciences* (BG), 13, 989–1007, <https://doi.org/10.5194/bg-13-989-2016>,
1073 2016.
- 1074 Engel, A. and Händel, N.: A novel protocol for determining the concentration and composition of sugars in particulate and in
1075 high molecular weight dissolved organic matter (HMW-DOM) in seawater, *Marine Chemistry*, 127, 180–191,
1076 <https://doi.org/10.1016/j.marchem.2011.09.004>, 2011.
- 1077 Engel, A., Thoms, S., Riebesell, U., Rochelle-Newall, E., and Zondervan, I.: Polysaccharide aggregation as a potential sink of
1078 marine dissolved organic carbon, *Nature*, 428, 929–932, <https://doi.org/10.1038/nature02453>, 2004.
- 1079 Engel, A., Harlay, J., Piontek, J., and Chou, L.: Contribution of combined carbohydrates to dissolved and particulate organic
1080 carbon after the spring bloom in the northern Bay of Biscay (North-Eastern Atlantic Ocean), *Continental Shelf Research*, 45,
1081 42–53, <https://doi.org/10.1016/j.csr.2012.05.016>, 2012.
- 1082 Ervens, B. and Amato, P.: The global impact of bacterial processes on carbon mass, *Atmospheric Chemistry & Physics*, 20,
1083 1777–1794, <https://doi.org/10.5194/acp-20-1777-2020>, 2020.
- 1084 Esau, I. and Repina, I.: Wind Climate in Kongsfjorden, Svalbard, and Attribution of Leading Wind Driving Mechanisms through
1085 Turbulence-Resolving Simulations, *Advances in Meteorology*, 2012, 568454, <https://doi.org/10.1155/2012/568454>, 2012.
- 1086 Fabiano, M., Povero, P., and Danovaro, R.: Distribution and composition of particulate organic matter in the Ross Sea
1087 (Antarctica), *Polar Biol*, 13, 525–533, <https://doi.org/10.1007/BF00236394>, 1993.
- 1088 Facchini, M. C., Rinaldi, M., Decesari, S., Carbone, C., Finessi, E., Mircea, M., Fuzzi, S., Ceburnis, D., Flanagan, R., Nilsson, E. D.,
1089 Leeuw, G. de, Martino, M., Woeltjen, J., and O’Dowd, C. D.: Primary submicron marine aerosol dominated by insoluble organic
1090 colloids and aggregates, *Geophysical Research Letters*, 35, 1–5, <https://doi.org/10.1029/2008GL034210>, 2008.
- 1091 Farmer, D. K., Cappa, C. D., and Kreidenweis, S. M.: Atmospheric Processes and Their Controlling Influence on Cloud
1092 Condensation Nuclei Activity, *Chem. Rev.*, 115, 4199–4217, <https://doi.org/10.1021/cr5006292>, 2015.
- 1093 Farmer, D. K., Boedicker, E. K., and DeBolt, H. M.: Dry Deposition of Atmospheric Aerosols: Approaches, Observations, and
1094 Mechanisms, *Annual Review of Physical Chemistry*, 72, 375–397, <https://doi.org/10.1146/annurev-physchem-090519-034936>, 2021.
- 1096 Feltracco, M., Barbaro, E., Hoppe, C. J. M., Wolf, K. K. E., Spolaor, A., Layton, R., Keuschnig, C., Barbante, C., Gambaro, A., and
1097 Larose, C.: Airborne bacteria and particulate chemistry capture Phytoplankton bloom dynamics in an Arctic fjord, *Atmospheric*
1098 *Environment*, 256, 118458, <https://doi.org/10.1016/j.atmosenv.2021.118458>, 2021.
- 1099 Fomba, K. W., Müller, K., van Pinxteren, D., Poulain, L., van Pinxteren, M., and Herrmann, H.: Long-term chemical
1100 characterization of tropical and marine aerosols at the Cape Verde Atmospheric Observatory (CVAO) from 2007 to 2011,
1101 *Atmospheric Chemistry and Physics*, 14, 8883–8904, <https://doi.org/10.5194/acp-14-8883-2014>, 2014.
- 1102 Francis, J. A. and Wu, B.: Why has no new record-minimum Arctic sea-ice extent occurred since September 2012?, *Environ.*
1103 *Res. Lett.*, 15, 114034, <https://doi.org/10.1088/1748-9326/abc047>, 2020.
- 1104 Freud, E., Krejci, R., Tunved, P., Leaitch, R., Nguyen, Q. T., Massling, A., Skov, H., and Barrie, L.: Pan-Arctic aerosol number size
1105 distributions: seasonality and transport patterns, *Atmospheric Chemistry and Physics*, 17, 8101–8128,
1106 <https://doi.org/10.5194/acp-17-8101-2017>, 2017.
- 1107 Gantt, B., Meskhidze, N., Facchini, M. C., Rinaldi, M., Ceburnis, D., and O’Dowd, C. D.: Wind speed dependent size-resolved
1108 parameterization for the organic mass fraction of sea spray aerosol, *Atmospheric Chemistry and Physics*, 11, 8777–8790,
1109 <https://doi.org/10.5194/acp-11-8777-2011>, 2011.
- 1110 Gao, Q., Leck, C., Rauschenberg, C., and Matrai, P. A.: On the chemical dynamics of extracellular polysaccharides in the high
1111 Arctic surface microlayer, *Ocean Science*, 8, 401–418, <https://doi.org/10.5194/os-8-401-2012>, 2012.
- 1112 Gierens, R., Kneifel, S., Shupe, M. D., Ebell, K., Maturilli, M., and Löhnert, U.: Low-level mixed-phase clouds in a complex Arctic
1113 environment, *Atmospheric Chemistry and Physics*, 20, 3459–3481, <https://doi.org/10.5194/acp-20-3459-2020>, 2020.
- 1114 Goldberg, S. J., Carlson, C. A., Brzezinski, M., Nelson, N. B., and Siegel, D. A.: Systematic removal of neutral sugars within
1115 dissolved organic matter across ocean basins, *Geophysical Research Letters*, 38, 1–7,
1116 <https://doi.org/10.1029/2011GL048620>, 2011.



- 1117 Grawe, S., Jentzsch, C., Schaefer, J., Wex, H., Mertes, S., and Stratmann, F.: Next-generation ice-nucleating particle sampling
1118 on board aircraft: characterization of the High-volume flow aERosol particle filter sAMpler (HERA), *Atmospheric Measurement*
1119 *Techniques*, 16, 4551–4570, <https://doi.org/10.5194/amt-16-4551-2023>, 2023.
- 1120 Grolmund, G. and Wickham, H.: Dates and Times Made Easy with lubridate, *Journal of Statistical Software*, 40, 1–25, 2011.
- 1121 Grosse, J., Nöthig, E.-M., Torres-Valdés, S., and Engel, A.: Summertime Amino Acid and Carbohydrate Patterns in Particulate
1122 and Dissolved Organic Carbon Across Fram Strait, *Front. Mar. Sci.*, 8, <https://doi.org/10.3389/fmars.2021.684675>, 2021.
- 1123 Guo, T., Li, K., Zhu, Y., Gao, H., and Yao, X.: Concentration and size distribution of particulate oxalate in marine and coastal
1124 atmospheres – Implication for the increased importance of oxalate in nanometer atmospheric particles, *Atmospheric*
1125 *Environment*, 142, 19–31, <https://doi.org/10.1016/j.atmosenv.2016.07.026>, 2016.
- 1126 Gürses, Ö., Oziel, L., Karakuş, O., Sidorenko, D., Völker, C., Ye, Y., Zeising, M., Butzin, M., and Hauck, J.: Ocean biogeochemistry
1127 in the coupled ocean–sea ice–biogeochemistry model FESOM2.1–REcoM3, *Geoscientific Model Development*, 16, 4883–
1128 4936, <https://doi.org/10.5194/gmd-16-4883-2023>, 2023.
- 1129 Haddrell, A. E. and Thomas, R. J.: Aerobiology: Experimental Considerations, Observations, and Future Tools, *Appl. Environ.*
1130 *Microbiol.*, 83, 1–15, <https://doi.org/10.1128/AEM.00809-17>, 2017.
- 1131 Hansell, D. A.: Recalcitrant Dissolved Organic Carbon Fractions, *Annual Review of Marine Science*, 5, 421–445,
1132 <https://doi.org/10.1146/annurev-marine-120710-100757>, 2013.
- 1133 Hara, K., Yamagata, S., Yamanouchi, T., Sato, K., Herber, A., Iwasaka, Y., Nagatani, M., and Nakata, H.: Mixing states of
1134 individual aerosol particles in spring Arctic troposphere during ASTAR 2000 campaign, *Journal of Geophysical Research:*
1135 *Atmospheres*, 108, 1–12, <https://doi.org/10.1029/2002JD002513>, 2003.
- 1136 Hartmann, S., Schrödner, R., Hassett, B. T., Hartmann, M., van Pinxteren, M., Fomba, K. W., Stratmann, F., Herrmann, H.,
1137 Pöhlker, M., and Zeppenfeld, S.: Polysaccharides–Important Constituents of Ice-Nucleating Particles of Marine Origin,
1138 *Environ. Sci. Technol.*, 59, 5098–5108, <https://doi.org/10.1021/acs.est.4c08014>, 2025.
- 1139 Hasenecz, E., Jayarathne, T., Pendergraft, M. A., Santander, M. V., Mayer, K. J., Sauer, J., Lee, C., Gibson, W. S., Kruse, S. M.,
1140 Malfatti, F., Prather, K. A., and Stone, E. A.: Marine bacteria affect saccharide enrichment in sea spray aerosol during a
1141 phytoplankton bloom, *ACS Earth Space Chem.*, 4, 1638–1649, <https://doi.org/10.1021/acsearthspacechem.0c00167>, 2020.
- 1142 Hasenecz, E. S., Kaluarachchi, C. P., Lee, H. D., Tivanski, A. V., and Stone, E. A.: Saccharide Transfer to Sea Spray Aerosol
1143 Enhanced by Surface Activity, Calcium, and Protein Interactions, *ACS Earth Space Chem.*, 3, 2539–2548,
1144 <https://doi.org/10.1021/acsearthspacechem.9b00197>, 2019.
- 1145 Herrmann, H., Tilgner, A., Barzaghi, P., Majdik, Z., Gligorovski, S., Poulain, L., and Monod, A.: Towards a more detailed
1146 description of tropospheric aqueous phase organic chemistry: CAPRAM 3.0, *Atmospheric Environment*, 39, 4351–4363,
1147 <https://doi.org/10.1016/j.atmosenv.2005.02.016>, 2005.
- 1148 Heutte, B., Bergner, N., Angot, H., Pernov, J. B., Dada, L., Mirrielees, J. A., Beck, I., Baccarini, A., Boyer, M., Creamean, J. M.,
1149 Daellenbach, K. R., El Haddad, I., Frey, M. M., Henning, S., Laurila, T., Moschos, V., Petäjä, T., Pratt, K. A., Quéléver, L. L. J.,
1150 Shupe, M. D., Zieger, P., Jokinen, T., and Schmale, J.: Observations of high-time-resolution and size-resolved aerosol chemical
1151 composition and microphysics in the central Arctic: implications for climate-relevant particle properties, *Atmospheric*
1152 *Chemistry and Physics*, 25, 2207–2241, <https://doi.org/10.5194/acp-25-2207-2025>, 2025.
- 1153 Hijmans, R. J.: raster: Geographic Data Analysis and Modeling, R package version 3.6-26, 2023.
- 1154 Hill, T. C. J., Malfatti, F., McCluskey, C. S., Schill, G. P., Santander, M. V., Moore, K. A., Rauker, A. M., Perkins, R. J., Celussi, M.,
1155 Levin, E. J. T., Suski, K. J., Cornwell, G. C., Lee, C., Negro, P. D., Kreidenweis, S. M., Prather, K. A., and DeMott, P. J.: Resolving
1156 the controls over the production and emission of ice-nucleating particles in sea spray, *Environ. Sci.: Atmos.*,
1157 <https://doi.org/10.1039/D2EA00154C>, 2023.
- 1158 Hoffman, E. J. and Duce, R. A.: Factors influencing the organic carbon content of marine aerosols: A laboratory study, *Journal*
1159 *of Geophysical Research (1896-1977)*, 81, 3667–3670, <https://doi.org/10.1029/JC081i021p03667>, 1976.
- 1160 Hogan, R. J., Mittermaier, M. P., and Illingworth, A. J.: The Retrieval of Ice Water Content from Radar Reflectivity Factor and
1161 Temperature and Its Use in Evaluating a Mesoscale Model, *Journal of Applied Meteorology and Climatology*, 45, 301–317,
1162 <https://doi.org/10.1175/JAM2340.1>, 2006.
- 1163 Hoppel, W. A., Frick, G. M., and Fitzgerald, J. W.: Surface source function for sea-salt aerosol and aerosol dry deposition to
1164 the ocean surface, *Journal of Geophysical Research: Atmospheres*, 107, AAC 7-1–AAC 7-17,
1165 <https://doi.org/10.1029/2001JD002014>, 2002.
- 1166 Illingworth, A. J., Hogan, R. J., O'Connor, E. J., Bouniol, D., Brooks, M. E., Delanoé, J., Donovan, D. P., Eastment, J. D., Gaussiat,
1167 N., Goddard, J. W. F., Haeffelin, M., Baltink, H. K., Krasnov, O. A., Pelon, J., Piriou, J.-M., Protat, A., Russchenberg, H. W. J.,
1168 Seifert, A., Tompkins, A. M., Zadelhoff, G.-J. van, Vinit, F., Willén, U., Wilson, D. R., and Wrench, C. L.: Cloudnet: Continuous
1169 Evaluation of Cloud Profiles in Seven Operational Models Using Ground-Based Observations, *Bulletin of the American*
1170 *Meteorological Society*, 88, 883–898, <https://doi.org/10.1175/BAMS-88-6-883>, 2007.



- 1171 Ittekkot, V., Brockmann, U., Michaelis, W., and Degens, E. T.: Dissolved free and combined carbohydrates during a
1172 phytoplankton bloom in the northern North Sea, *Marine Ecology Progress Series*, 4, 299–305, 1981.
- 1173 Jayarathne, T., Sultana, C. M., Lee, C., Malfatti, F., Cox, J. L., Pendergraft, M. A., Moore, K. A., Azam, F., Tivanski, A. V., Cappa,
1174 C. D., Bertram, T. H., Grassian, V. H., Prather, K. A., and Stone, E. A.: Enrichment of Saccharides and Divalent Cations in Sea
1175 Spray Aerosol During Two Phytoplankton Blooms, *Environ Sci Technol*, 50, 11511–11520,
1176 <https://doi.org/10.1021/acs.est.6b02988>, 2016.
- 1177 Jensen, L. Z., Glasius, M., Gryning, S.-E., Massling, A., Finster, K., and Šantl-Temkiv, T.: Seasonal Variation of the Atmospheric
1178 Bacterial Community in the Greenlandic High Arctic Is Influenced by Weather Events and Local and Distant Sources, *Front.*
1179 *Microbiol.*, 13, <https://doi.org/10.3389/fmicb.2022.909980>, 2022.
- 1180 Kang, H., Jung, C. H., Lee, B. Y., Krejci, R., Heslin-Rees, D., Aas, W., and Yoon, Y. J.: Aerosol hygroscopicity influenced by
1181 seasonal chemical composition variations in the Arctic region, *Journal of Aerosol Science*, 106551,
1182 <https://doi.org/10.1016/j.jaerosci.2025.106551>, 2025.
- 1183 Kanji, Z. A., Ladino, L. A., Wex, H., Boose, Y., Burkert-Kohn, M., Cziczo, D. J., and Krämer, M.: Overview of Ice Nucleating
1184 Particles, *Meteorological Monographs*, 58, 1.1-1.33, <https://doi.org/10.1175/AMSMONOGRAPH5-D-16-0006.1>, 2017.
- 1185 Karl, M., Leck, C., Rad, F. M., Bäcklund, A., Lopez-Aparicio, S., and Heintzenberg, J.: New insights in sources of the sub-
1186 micrometre aerosol at Mt. Zeppelin observatory (Spitsbergen) in the year 2015, *Tellus B: Chemical and Physical Meteorology*,
1187 71, 1613143, <https://doi.org/10.1080/16000889.2019.1613143>, 2019.
- 1188 Kawamura, K. and Bikkina, S.: A review of dicarboxylic acids and related compounds in atmospheric aerosols: Molecular
1189 distributions, sources and transformation, *Atmospheric Research*, 170, 140–160,
1190 <https://doi.org/10.1016/j.atmosres.2015.11.018>, 2016.
- 1191 Kawamura, K., Kasukabe, H., and Barrie, L. A.: Source and reaction pathways of dicarboxylic acids, ketoacids and dicarbonyls
1192 in arctic aerosols: One year of observations, *Atmospheric Environment*, 30, 1709–1722, [https://doi.org/10.1016/1352-2310\(95\)00395-9](https://doi.org/10.1016/1352-2310(95)00395-9), 1996a.
- 1194 Kawamura, K., Sempéré, R., Imai, Y., Fujii, Y., and Hayashi, M.: Water soluble dicarboxylic acids and related compounds in
1195 Antarctic aerosols, *Journal of Geophysical Research: Atmospheres*, 101, 18721–18728, <https://doi.org/10.1029/96JD01541>,
1196 1996b.
- 1197 Keene, W. C., Pszenny, A. A. P., Galloway, J. N., and Hawley, M. E.: Sea-salt corrections and interpretation of constituent ratios
1198 in marine precipitation, *Journal of Geophysical Research*, 91, 6647–6658, <https://doi.org/10.1029/JD091iD06p06647>, 1986.
- 1199 Keene, W. C., Long, M. S., Reid, J. S., Frossard, A. A., Kieber, D. J., Maben, J. R., Russell, L. M., Kinsey, J. D., Quinn, P. K., and
1200 Bates, T. S.: Factors That Modulate Properties of Primary Marine Aerosol Generated From Ambient Seawater on Ships at Sea,
1201 *Journal of Geophysical Research: Atmospheres*, 122, 11,961–11,990, <https://doi.org/10.1002/2017JD026872>, 2017.
- 1202 Kerminen, V.-M., Teinilä, K., Hillamo, R., and Mäkelä, T.: Size-segregated chemistry of particulate dicarboxylic acids in the
1203 Arctic atmosphere, *Atmospheric Environment*, 33, 2089–2100, [https://doi.org/10.1016/S1352-2310\(98\)00350-1](https://doi.org/10.1016/S1352-2310(98)00350-1), 1999.
- 1204 Khadem, H. E.: *Carbohydrate Chemistry: Monosaccharides and Their Oligomers*, Elsevier, 267 pp., 2012.
- 1205 Kharbush, J. J., Close, H. G., Van Mooy, B. A. S., Arnosti, C., Smittenberg, R. H., Le Moigne, F. A. C., Mollenhauer, G., Scholz-
1206 Böttcher, B., Obrecht, I., Koch, B. P., Becker, K., Iversen, M. H., and Mohr, W.: Particulate Organic Carbon Deconstructed:
1207 Molecular and Chemical Composition of Particulate Organic Carbon in the Ocean, *Frontiers in Marine Science*, 7, Art.Nr. 518,
1208 <https://doi.org/10.3389/fmars.2020.00518>, 2020.
- 1209 Kirchman, D. L., Meon, B., Ducklow, H. W., Carlson, C. A., Hansell, D. A., and Steward, G. F.: Glucose fluxes and concentrations
1210 of dissolved combined neutral sugars (polysaccharides) in the Ross Sea and Polar Front Zone, Antarctica, *Deep Sea Research*
1211 *Part II: Topical Studies in Oceanography*, 48, 4179–4197, [https://doi.org/10.1016/S0967-0645\(01\)00085-6](https://doi.org/10.1016/S0967-0645(01)00085-6), 2001.
- 1212 Klein, A. M., Bohannon, B. J. M., Jaffe, D. A., Levin, D. A., and Green, J. L.: Molecular Evidence for Metabolically Active Bacteria
1213 in the Atmosphere, *Front. Microbiol.*, 7, 772, <https://doi.org/10.3389/fmicb.2016.00772>, 2016.
- 1214 Köllner, F., Schneider, J., Willis, M. D., Klimach, T., Helleis, F., Bozem, H., Kunkel, D., Hoor, P., Burkart, J., Leaitch, W. R.,
1215 Aliabadi, A. A., Abbatt, J. P. D., Herber, A. B., and Borrmann, S.: Particulate trimethylamine in the summertime Canadian high
1216 Arctic lower troposphere, *Atmospheric Chemistry and Physics*, 17, 13747–13766, [https://doi.org/10.5194/acp-17-13747-](https://doi.org/10.5194/acp-17-13747-2017)
1217 2017, 2017.
- 1218 Leck, C., Gao, Q., Mashayekhy Rad, F., and Nilsson, U.: Size-resolved atmospheric particulate polysaccharides in the high
1219 summer Arctic, *Atmospheric Chemistry and Physics*, 13, 12573–12588, <https://doi.org/10.5194/acp-13-12573-2013>, 2013.
- 1220 Leon-Marcos, A., Zeising, M., van Pinxteren, M., Zeppenfeld, S., Bracher, A., Barbaro, E., Engel, A., Feltracco, M., Tegen, I., and
1221 Heinold, B.: Modelling emission and transport of key components of primary marine organic aerosol using the global aerosol-
1222 climate model ECHAM6.3–HAM2.3, *Geoscientific Model Development*, 18, 4183–4213, [https://doi.org/10.5194/gmd-18-](https://doi.org/10.5194/gmd-18-4183-2025)
1223 4183-2025, 2025.



- 1224 Li, J., Han, Z., Fu, P., Yao, X., and Liang, M.: Seasonal characteristics of emission, distribution, and radiative effect of marine
1225 organic aerosols over the western Pacific Ocean: an investigation with a coupled regional climate aerosol model, *Atmospheric*
1226 *Chemistry and Physics*, 24, 3129–3161, <https://doi.org/10.5194/acp-24-3129-2024>, 2024.
- 1227 Lohmann, U. and Feichter, J.: Global indirect aerosol effects: a review, *Atmospheric Chemistry and Physics*, 5, 715–737,
1228 <https://doi.org/10.5194/acp-5-715-2005>, 2005.
- 1229 Madry, W. L., Toon, O. B., and O'Dowd, C. D.: Modeled optical thickness of sea-salt aerosol, *Journal of Geophysical Research:*
1230 *Atmospheres*, 116, <https://doi.org/10.1029/2010JD014691>, 2011.
- 1231 Malfatti, F., Lee, C., Tinta, T., Pendergraft, M. A., Celussi, M., Zhou, Y., Sultana, C. M., Rotter, A., Axson, J. L., Collins, D. B.,
1232 Santander, M. V., Anides Morales, A. L., Aluwihare, L. I., Riemer, N., Grassian, V. H., Azam, F., and Prather, K. A.: Detection of
1233 Active Microbial Enzymes in Nascent Sea Spray Aerosol: Implications for Atmospheric Chemistry and Climate, *Environ. Sci.*
1234 *Technol. Lett.*, 6, 171–177, <https://doi.org/10.1021/acs.estlett.8b00699>, 2019.
- 1235 Manders, A. M. M., Schaap, M., Querol, X., Albert, M. F. M. A., Vercauteren, J., Kuhlbusch, T. A. J., and Hoogerbrugge, R.: Sea
1236 salt concentrations across the European continent, *Atmospheric Environment*, 44, 2434–2442,
1237 <https://doi.org/10.1016/j.atmosenv.2010.03.028>, 2010.
- 1238 Matulová, M., Husárová, S., Capek, P., Sancelme, M., and Delort, A.-M.: Biotransformation of Various Saccharides and
1239 Production of Exopolymeric Substances by Cloud-Borne *Bacillus* sp. 3B6, *Environ. Sci. Technol.*, 48, 14238–14247,
1240 <https://doi.org/10.1021/es501350s>, 2014.
- 1241 Maturilli, M.: Continuous meteorological observations at station Ny-Ålesund (2011-08 et seq), Alfred Wegener Institute -
1242 Research Unit Potsdam, <https://doi.org/10.1594/PANGAEA.914979>, 2020.
- 1243 Maturilli, M., Herber, A., and König-Langlo, G.: Climatology and time series of surface meteorology in Ny-Ålesund, Svalbard,
1244 *Earth System Science Data*, 5, 155–163, <https://doi.org/10.5194/essd-5-155-2013>, 2013.
- 1245 Maturilli, M., Herber, A., and König-Langlo, G.: Surface radiation climatology for Ny-Ålesund, Svalbard (78.9° N), basic
1246 observations for trend detection, *Theor Appl Climatol*, 120, 331–339, <https://doi.org/10.1007/s00704-014-1173-4>, 2015.
- 1247 Mayot, N., Matrai, P., Ellingsen, I. H., Steele, M., Johnson, K., Riser, S. C., and Swift, D.: Assessing Phytoplankton Activities in
1248 the Seasonal Ice Zone of the Greenland Sea Over an Annual Cycle, *Journal of Geophysical Research: Oceans*, 123, 8004–8025,
1249 <https://doi.org/10.1029/2018JC014271>, 2018.
- 1250 McNeill, V. F.: Aqueous Organic Chemistry in the Atmosphere: Sources and Chemical Processing of Organic Aerosols, *Environ.*
1251 *Sci. Technol.*, 49, 1237–1244, <https://doi.org/10.1021/es5043707>, 2015.
- 1252 Mirrielees, J. A., Kirpes, R. M., Costa, E. J., Porter, G. C. E., Murray, B. J., Lata, N. N., Boschi, V., China, S., Grannas, A. M., Ault,
1253 A. P., Matrai, P. A., and Pratt, K. A.: Marine aerosol generation experiments in the High Arctic during summertime, *Elementa:*
1254 *Science of the Anthropocene*, 12, 00134, <https://doi.org/10.1525/elementa.2023.00134>, 2024.
- 1255 Müller, K., Lehmann, S., Pinxteren, D. van, Gnauk, T., Niedermeier, N., Wiedensohler, A., and Herrmann, H.: Particle
1256 characterization at the Cape Verde atmospheric observatory during the 2007 RHaMBLe intensive, *Atmospheric Chemistry*
1257 *and Physics*, 10, 2709–2721, <https://doi.org/10.5194/acp-10-2709-2010>, 2010.
- 1258 Neuwirth, E.: RColorBrewer: ColorBrewer Palettes, R package version 1.1-3, 2022.
- 1259 Nomokonova, T., Ebell, K., Löhnert, U., Maturilli, M., Ritter, C., and O'Connor, E.: Statistics on clouds and their relation to
1260 thermodynamic conditions at Ny-Ålesund using ground-based sensor synergy, *Atmospheric Chemistry and Physics*, 19, 4105–
1261 4126, <https://doi.org/10.5194/acp-19-4105-2019>, 2019.
- 1262 O'Dowd, C. D. and de Leeuw, G.: Marine aerosol production: a review of the current knowledge, *Philos Trans A Math Phys*
1263 *Eng Sci*, 365, 1753–1774, <https://doi.org/10.1098/rsta.2007.2043>, 2007.
- 1264 O'Dowd, C. D., Smith, M. H., Consterdine, I. E., and Lowe, J. A.: Marine aerosol, sea-salt, and the marine sulphur cycle: a short
1265 review, *Atmospheric Environment*, 31, 73–80, [https://doi.org/10.1016/S1352-2310\(96\)00106-9](https://doi.org/10.1016/S1352-2310(96)00106-9), 1997.
- 1266 Ooki, A., Uematsu, M., Miura, K., and Nakae, S.: Sources of sodium in atmospheric fine particles, *Atmospheric Environment*,
1267 36, 4367–4374, [https://doi.org/10.1016/S1352-2310\(02\)00341-2](https://doi.org/10.1016/S1352-2310(02)00341-2), 2002.
- 1268 Orellana, M. V. and Leck, C.: Chapter 9 - Marine Microgels, in: *Biogeochemistry of Marine Dissolved Organic Matter* (Second
1269 Edition), edited by: Hansell, D. A. and Carlson, C. A., Academic Press, Boston, 451–480, <https://doi.org/10.1016/B978-0-12-405940-5.00009-1>, 2015.
- 1271 Orellana, M. V., Matrai, P. A., Leck, C., Rauschenberg, C. D., Lee, A. M., and Coz, E.: Marine microgels as a source of cloud
1272 condensation nuclei in the high Arctic, *PNAS*, 108, 13612–13617, <https://doi.org/10.1073/pnas.1102457108>, 2011.
- 1273 Oziel, L., Schourup-Kristensen, V., Wekerle, C., and Hauck, J.: The Pan-Arctic Continental Slope as an Intensifying Conveyor
1274 Belt for Nutrients in the Central Arctic Ocean (1985–2015), *Global Biogeochemical Cycles*, 36, e2021GB007268,
1275 <https://doi.org/10.1029/2021GB007268>, 2022.



- 1276 Panagiotopoulos, C. and Sempéré, R.: Analytical methods for the determination of sugars in marine samples: A historical
1277 perspective and future directions, *Limnology and Oceanography: Methods*, 3, 419–454,
1278 <https://doi.org/10.4319/lom.2005.3.419>, 2005.
- 1279 Penner, J. E., Andreae, M. O., Annegarn, H., Barrie, L., Feichter, J., Hegg, D., Jayaraman, A., Leaitch, R., Murphy, D., Nganga,
1280 J., and Pitari, G.: Aerosols, their Direct and Indirect Effects, *Climate Change 2001: The Scientific Basis. Contribution of Working*
1281 *Group I to the Third Assessment Report of the Intergovernmental Panel on Climate Change*, 289–348, 2001.
- 1282 Pierce, D.: ncd4: Interface to Unidata netCDF (Version 4 or Earlier) Format Data, R package version 1.22, 2023.
- 1283 Pilinis, C., Pandis, S. N., and Seinfeld, J. H.: Sensitivity of direct climate forcing by atmospheric aerosols to aerosol size and
1284 composition, *Journal of Geophysical Research*, 100, 18,739–18,754, <https://doi.org/10.1029/95JD02119>, 1995.
- 1285 Pilz, C., Düsing, S., Wehner, B., Müller, T., Siebert, H., Voigtländer, J., and Lonardi, M.: CAMP: an instrumented platform for
1286 balloon-borne aerosol particle studies in the lower atmosphere, *Atmospheric Measurement Techniques*, 15, 6889–6905,
1287 <https://doi.org/10.5194/amt-15-6889-2022>, 2022.
- 1288 Pilz, C., Lonardi, M., Egerer, U., Siebert, H., Ehrlich, A., Heymsfield, A. J., Schmitt, C. G., Shupe, M. D., Wehner, B., and
1289 Wendisch, M.: Profile observations of the Arctic atmospheric boundary layer with the BELUGA tethered balloon during
1290 MOSAiC, *Sci Data*, 10, 534, <https://doi.org/10.1038/s41597-023-02423-5>, 2023.
- 1291 Pilz, C., Cassano, J. J., de Boer, G., Kirbus, B., Lonardi, M., Pöhlker, M., Shupe, M. D., Siebert, H., Wendisch, M., and Wehner,
1292 B.: Tethered balloon measurements reveal enhanced aerosol occurrence aloft interacting with Arctic low-level clouds,
1293 *Elementa: Science of the Anthropocene*, 12, 00120, <https://doi.org/10.1525/elementa.2023.00120>, 2024.
- 1294 van Pinxteren, M., Müller, C., Iinuma, Y., Stolle, C., and Herrmann, H.: Chemical Characterization of Dissolved Organic
1295 Compounds from Coastal Sea Surface Microlayers (Baltic Sea, Germany), *Environmental Science & Technology*, 46, 10455–
1296 10462, <https://doi.org/10.1021/es204492b>, 2012.
- 1297 van Pinxteren, M., Barthel, S., Fomba, K. W., Müller, K., Von Tümpling, W., and Herrmann, H.: The influence of environmental
1298 drivers on the enrichment of organic carbon in the sea surface microlayer and in submicron aerosol particles – measurements
1299 from the Atlantic Ocean, *Elem Sci Anth*, 5, 1–21, <https://doi.org/10.1525/elementa.225>, 2017.
- 1300 van Pinxteren, M., Robinson, T.-B., Zeppenfeld, S., Gong, X., Bahlmann, E., Fomba, K. W., Triesch, N., Stratmann, F., Wurl, O.,
1301 Engel, A., Wex, H., and Herrmann, H.: High number concentrations of transparent exopolymer particles in ambient aerosol
1302 particles and cloud water – a case study at the tropical Atlantic Ocean, *Atmospheric Chemistry and Physics*, 22, 5725–5742,
1303 <https://doi.org/10.5194/acp-22-5725-2022>, 2022.
- 1304 van Pinxteren, M., Zeppenfeld, S., Fomba, K. W., Triesch, N., Frka, S., and Herrmann, H.: Amino acids, carbohydrates, and
1305 lipids in the tropical oligotrophic Atlantic Ocean: sea-to-air transfer and atmospheric in situ formation, *Atmospheric Chemistry*
1306 *and Physics*, 23, 6571–6590, <https://doi.org/10.5194/acp-23-6571-2023>, 2023.
- 1307 Platt, S. M., Hov, Ø., Berg, T., Breivik, K., Eckhardt, S., Eleftheriadis, K., Evangeliou, N., Fiebig, M., Fisher, R., Hansen, G.,
1308 Hansson, H.-C., Heintzenberg, J., Hermansen, O., Heslin-Rees, D., Holmén, K., Hudson, S., Kallenborn, R., Krejci, R., Krognes,
1309 T., Larssen, S., Lowry, D., Lund Myhre, C., Lunder, C., Nisbet, E., Nizzetto, P. B., Park, K.-T., Pedersen, C. A., Aspmo Pfaffhuber,
1310 K., Röckmann, T., Schmidbauer, N., Solberg, S., Stohl, A., Ström, J., Svendby, T., Tunved, P., Tørnkvist, K., van der Veen, C.,
1311 Vratolis, S., Yoon, Y. J., Yttri, K. E., Zieger, P., Aas, W., and Tørseth, K.: Atmospheric composition in the European Arctic and
1312 30 years of the Zeppelin Observatory, Ny-Ålesund, *Atmospheric Chemistry and Physics*, 22, 3321–3369,
1313 <https://doi.org/10.5194/acp-22-3321-2022>, 2022.
- 1314 van de Poll, W. H., Maat, D. S., Fischer, P., Visser, R. J. W., Brussaard, C. P. D., and Buma, A. G. J.: Solar radiation and solar
1315 radiation driven cycles in warming and freshwater discharge control seasonal and inter-annual phytoplankton chlorophyll a
1316 and taxonomic composition in a high Arctic fjord (Kongsfjorden, Spitsbergen), *Limnology and Oceanography*, 66, 1221–1236,
1317 <https://doi.org/10.1002/lno.11677>, 2021.
- 1318 Porter, G. C. E., Adams, M. P., Brooks, I. M., Ickes, L., Karlsson, L., Leck, C., Salter, M. E., Schmale, J., Siegel, K., Sikora, S. N. F.,
1319 Tarn, M. D., Vüllers, J., Wernli, H., Zieger, P., Zinke, J., and Murray, B. J.: Highly Active Ice-Nucleating Particles at the Summer
1320 North Pole, *Journal of Geophysical Research: Atmospheres*, 127, e2021JD036059, <https://doi.org/10.1029/2021JD036059>,
1321 2022.
- 1322 Quinn, P. K., Collins, D. B., Grassian, V. H., Prather, K. A., and Bates, T. S.: Chemistry and Related Properties of Freshly Emitted
1323 Sea Spray Aerosol, *Chemical Reviews*, 115, 4383–4399, <https://doi.org/10.1021/cr500713g>, 2015.
- 1324 Ramasamy, K. P., Mahawar, L., Rajasabapathy, R., Rajeshwari, K., Miceli, C., and Pucciarelli, S.: Comprehensive insights on
1325 environmental adaptation strategies in Antarctic bacteria and biotechnological applications of cold adapted molecules, *Front.*
1326 *Microbiol.*, 14, <https://doi.org/10.3389/fmicb.2023.1197797>, 2023.
- 1327 Rinaldi, M., Decesari, S., Carbone, C., Finessi, E., Fuzzi, S., Ceburnis, D., O'Dowd, C. D., Sciare, J., Burrows, J. P., Vrekoussis, M.,
1328 Ervens, B., Tsigaridis, K., and Facchini, M. C.: Evidence of a natural marine source of oxalic acid and a possible link to glyoxal,
1329 *Journal of Geophysical Research: Atmospheres*, 116, <https://doi.org/10.1029/2011JD015659>, 2011.
- 1330 Robinson, T.-B., Stolle, C., and Wurl, O.: Depth is relative: the importance of depth for transparent exopolymer particles in
1331 the near-surface environment, *Ocean Science*, 15, 1653–1666, <https://doi.org/10.5194/os-15-1653-2019>, 2019a.



- 1332 Robinson, T.-B., Wurl, O., Bahlmann, E., Jürgens, K., and Stolle, C.: Rising bubbles enhance the gelatinous nature of the air–
1333 sea interface, *Limnology and Oceanography*, 64, 2358–2372, <https://doi.org/10.1002/lno.11188>, 2019b.
- 1334 Rocchi, A., von Jackowski, A., Welti, A., Li, G., Kanji, Z. A., Povazhnyy, V., Engel, A., Schmale, J., Nenes, A., Berdalet, E., Simó,
1335 R., and Dall’Osto, M.: Glucose Enhances Salinity-Driven Sea Spray Aerosol Production in Eastern Arctic Waters, *Environ. Sci.*
1336 *Technol.*, 58, 8748–8759, <https://doi.org/10.1021/acs.est.4c02826>, 2024.
- 1337 Russell, L. M., Hawkins, L. N., Frossard, A. A., Quinn, P. K., and Bates, T. S.: Carbohydrate-like composition of submicron
1338 atmospheric particles and their production from ocean bubble bursting, *Proc. Natl. Acad. Sci. U.S.A.*, 107, 6652–6657,
1339 <https://doi.org/10.1073/pnas.0908905107>, 2010.
- 1340 Sander, R., Keene, W. C., Pszenny, A. a. P., Arimoto, R., Ayers, G. P., Baboukas, E., Cainey, J. M., Crutzen, P. J., Duce, R. A.,
1341 Hönninger, G., Huebert, B. J., Maenhaut, W., Mihalopoulos, N., Turekian, V. C., and Van Dingenen, R.: Inorganic bromine in
1342 the marine boundary layer: a critical review, *Atmospheric Chemistry and Physics*, 3, 1301–1336, <https://doi.org/10.5194/acp-3-1301-2003>, 2003.
- 1344 Šantl-Temkiv, T., Gosewinkel, U., Starnawski, P., Lever, M., and Finster, K.: Aeolian dispersal of bacteria in southwest
1345 Greenland: their sources, abundance, diversity and physiological states, *FEMS Microbiol Ecol*, 94,
1346 <https://doi.org/10.1093/femsec/fiy031>, 2018.
- 1347 Šantl-Temkiv, T., Amato, P., Casamayor, E. O., Lee, P. K. H., and Pointing, S. B.: Microbial ecology of the atmosphere, *FEMS*
1348 *Microbiology Reviews*, 46, fuac009, <https://doi.org/10.1093/femsre/fuac009>, 2022.
- 1349 Schartau, M., Engel, A., Schröter, J., Thoms, S., Völker, C., and Wolf-Gladrow, D.: Modelling carbon overconsumption and the
1350 formation of extracellular particulate organic carbon, *Biogeosciences*, 4, 433–454, <https://doi.org/10.5194/bg-4-433-2007>,
1351 2007.
- 1352 Schill, S. R., Burrows, S. M., Hasenecz, E. S., Stone, E. A., and Bertram, T. H.: The Impact of Divalent Cations on the Enrichment
1353 of Soluble Saccharides in Primary Sea Spray Aerosol, *Atmosphere*, 9, 476, <https://doi.org/10.3390/atmos9120476>, 2018.
- 1354 Schmale, J., Zieger, P., and Ekman, A. M. L.: Aerosols in current and future Arctic climate, *Nature Climate Change*, 11, 95–105,
1355 <https://doi.org/10.1038/s41558-020-00969-5>, 2021.
- 1356 Schmale, J., Sharma, S., Decesari, S., Pernov, J., Massling, A., Hansson, H.-C., von Salzen, K., Skov, H., Andrews, E., Quinn, P.
1357 K., Upchurch, L. M., Eleftheriadis, K., Traversi, R., Gilardoni, S., Mazzola, M., Laing, J., and Hopke, P.: Pan-Arctic seasonal cycles
1358 and long-term trends of aerosol properties from 10 observatories, *Atmospheric Chemistry and Physics*, 22, 3067–3096,
1359 <https://doi.org/10.5194/acp-22-3067-2022>, 2022.
- 1360 Sharma, S., Barrie, L. a., Magnusson, E., Brattström, G., Leaith, W. r., Steffen, A., and Landsberger, S.: A Factor and Trends
1361 Analysis of Multidecadal Lower Tropospheric Observations of Arctic Aerosol Composition, Black Carbon, Ozone, and Mercury
1362 at Alert, Canada, *Journal of Geophysical Research: Atmospheres*, 124, 14133–14161, <https://doi.org/10.1029/2019JD030844>,
1363 2019.
- 1364 Shestakova, A., Chechin, D., Lüpkes, C., Hartmann, J., and Maturilli, M.: Foehn effect during easterly flow over Svalbard,
1365 <https://doi.org/10.5194/acp-2021-478>, 2021.
- 1366 Sinreich, R., Coburn, S., Dix, B., and Volkamer, R.: Ship-based detection of glyoxal over the remote tropical Pacific Ocean,
1367 *Atmospheric Chemistry and Physics*, 10, 11359–11371, <https://doi.org/10.5194/acp-10-11359-2010>, 2010.
- 1368 Sorooshian, A., Lu, M.-L., Brechtel, F. J., Jonsson, H., Feingold, G., Flagan, R. C., and Seinfeld, J. H.: On the Source of Organic
1369 Acid Aerosol Layers above Clouds, *Environ. Sci. Technol.*, 41, 4647–4654, <https://doi.org/10.1021/es0630442>, 2007.
- 1370 Stein, A. F., Draxler, R. R., Rolph, G. D., Stunder, B. J. B., Cohen, M. D., and Ngan, F.: NOAA’s HYSPLIT Atmospheric Transport
1371 and Dispersion Modeling System, *Bull. Amer. Meteor. Soc.*, 96, 2059–2077, <https://doi.org/10.1175/BAMS-D-14-00110.1>,
1372 2015.
- 1373 Struthers, H., Ekman, A. M. L., Glantz, P., Iversen, T., Kirkevåg, A., Mårtensson, E. M., Seland, Ø., and Nilsson, E. D.: The effect
1374 of sea ice loss on sea salt aerosol concentrations and the radiative balance in the Arctic, *Atmospheric Chemistry and Physics*,
1375 11, 3459–3477, <https://doi.org/10.5194/acp-11-3459-2011>, 2011.
- 1376 Su, B., Bi, X., Zhang, Z., Liang, Y., Song, C., Wang, T., Hu, Y., Li, L., Zhou, Z., Yan, J., Wang, X., and Zhang, G.: Enrichment of
1377 calcium in sea spray aerosol: insights from bulk measurements and individual particle analysis during the R/V *Xuelong* cruise
1378 in the summertime in Ross Sea, Antarctica, *Atmospheric Chemistry and Physics*, 23, 10697–10711,
1379 <https://doi.org/10.5194/acp-23-10697-2023>, 2023.
- 1380 Theodosi, C., Im, U., Bougiatioti, A., Zarnas, P., Yenigun, O., and Mihalopoulos, N.: Aerosol chemical composition over
1381 Istanbul, *Science of The Total Environment*, 408, 2482–2491, <https://doi.org/10.1016/j.scitotenv.2010.02.039>, 2010.
- 1382 Thyng, K., Greene, C. A., Hetland, R. D., Zimmerle, H. M., and DiMarco, S.: True colors of oceanography: Guidelines for effective
1383 and accurate colormap selection, *Oceanography*, 3, <https://doi.org/10.5670/oceanog.2016.66>, 2016.
- 1384 Tilgner, A. and Herrmann, H.: Radical-driven carbonyl-to-acid conversion and acid degradation in tropospheric aqueous
1385 systems studied by CAPRAM, *Atmospheric Environment*, 44, 5415–5422, <https://doi.org/10.1016/j.atmosenv.2010.07.050>,
1386 2010.



- 1387 Tørseth, K., Aas, W., Breivik, K., Fjæraa, A. M., Fiebig, M., Hjellbrekke, A. G., Lund Myhre, C., Solberg, S., and Yttri, K. E.:
 1388 Introduction to the European Monitoring and Evaluation Programme (EMEP) and observed atmospheric composition change
 1389 during 1972–2009, *Atmospheric Chemistry and Physics*, 12, 5447–5481, <https://doi.org/10.5194/acp-12-5447-2012>,
 1390 2012.
- 1391 Trainic, M., Koren, I., Sharoni, S., Frada, M., Segev, L., Rudich, Y., and Vardi, A.: Infection Dynamics of a Bloom-Forming Alga
 1392 and Its Virus Determine Airborne Coccolith Emission from Seawater, *iScience*, 6, 327–335,
 1393 <https://doi.org/10.1016/j.isci.2018.07.017>, 2018.
- 1394 Triesch, N., van Pinxteren, M., Engel, A., and Herrmann, H.: Concerted measurements of free amino acids at the Cabo Verde
 1395 islands: high enrichments in submicron sea spray aerosol particles and cloud droplets, *Atmospheric Chemistry and Physics*,
 1396 21, 163–181, <https://doi.org/10.5194/acp-21-163-2021>, 2021.
- 1397 Turekian, V. C., Macko, S. A., and Keene, W. C.: Concentrations, isotopic compositions, and sources of size-resolved,
 1398 particulate organic carbon and oxalate in near-surface marine air at Bermuda during spring, *Journal of Geophysical Research:*
 1399 *Atmospheres*, 108, <https://doi.org/10.1029/2002JD002053>, 2003.
- 1400 Veron, F.: Ocean Spray, *Annual Review of Fluid Mechanics*, 47, 507–538, [https://doi.org/10.1146/annurev-fluid-010814-](https://doi.org/10.1146/annurev-fluid-010814-014651)
 1401 014651, 2015.
- 1402 Vihtakari, M.: PlotSvalbard: PlotSvalbard-Plot research data from Svalbard on maps, R package version 0.9 2, 2020.
- 1403 Warneck, P.: In-cloud chemistry opens pathway to the formation of oxalic acid in the marine atmosphere, *Atmospheric*
 1404 *Environment*, 37, 2423–2427, [https://doi.org/10.1016/S1352-2310\(03\)00136-5](https://doi.org/10.1016/S1352-2310(03)00136-5), 2003.
- 1405 Wendisch, M., Brückner, M., Burrows, J. P., Crewell, S., Dethloff, K., Ebell, K., Lüpkes, C., Macke, A., Notholt, J., and Quaas, J.:
 1406 Understanding causes and effects of rapid warming in the Arctic, *Eos*, 98, 2017.
- 1407 Wendisch, M., Brückner, M., Crewell, S., Ehrlich, A., Notholt, J., Lüpkes, C., Macke, A., Burrows, J. P., Rinke, A., Quaas, J.,
 1408 Maturilli, M., Schemann, V., Shupe, M. D., Akansu, E. F., Barrientos-Velasco, C., Bärfuss, K., Blechschmidt, A.-M., Block, K.,
 1409 Bougoudis, I., Bozem, H., Böckmann, C., Bracher, A., Bresson, H., Bretschneider, L., Buschmann, M., Chechin, D. G., Chylik, J.,
 1410 Dahlke, S., Deneke, H., Dethloff, K., Donth, T., Dorn, W., Dupuy, R., Ebell, K., Egerer, U., Engelmann, R., Eppers, O., Gerdes, R.,
 1411 Gierens, R., Gorodetskaya, I. V., Gottschalk, M., Griesche, H., Gryanik, V. M., Handorf, D., Harm-Altstädter, B., Hartmann, J.,
 1412 Hartmann, M., Heinold, B., Herber, A., Herrmann, H., Heygster, G., Höschel, I., Hofmann, Z., Hölemann, J., Hünnerbein, A.,
 1413 Jafariserajehlou, S., Jäkel, E., Jacobi, C., Janout, M., Jansen, F., Jourdan, O., Jurányi, Z., Kalesse-Los, H., Kanzow, T., Käthner,
 1414 R., Kliesch, L. L., Klingebiel, M., Knudsen, E. M., Kovács, T., Körtke, W., Krampe, D., Kretzschmar, J., Kreyling, D., Kulla, B.,
 1415 Kunkel, D., Lampert, A., Lauer, M., Lelli, L., Lerber, A. von, Linke, O., Löhnert, U., Lonardi, M., Losa, S. N., Losch, M., Maahn,
 1416 M., Mech, M., Mei, L., Mertes, S., Metzner, E., Mewes, D., Michaelis, J., Mioche, G., Moser, M., Nakoudi, K., Neggers, R.,
 1417 Neuber, R., Nomokonova, T., Oelker, J., Papakonstantinou-Prsvelou, I., et al.: Atmospheric and Surface Processes, and
 1418 Feedback Mechanisms Determining Arctic Amplification: A Review of First Results and Prospects of the (AC)3 Project, *Bulletin*
 1419 *of the American Meteorological Society*, 104, E208–E242, <https://doi.org/10.1175/BAMS-D-21-0218.1>, 2023.
- 1420 White, W. H.: Chemical markers for sea salt in IMPROVE aerosol data, *Atmospheric Environment*, 42, 261–274,
 1421 <https://doi.org/10.1016/j.atmosenv.2007.09.040>, 2008.
- 1422 Wickham, H.: Reshaping Data with the reshape Package, *Journal of Statistical Software*, 21, 1–20, 2007.
- 1423 Wickham, H.: ggplot2: Elegant Graphics for Data Analysis, Springer-Verlag New York, [https://doi.org/10.1007/978-3-319-](https://doi.org/10.1007/978-3-319-24277-4_2)
 1424 24277-4_2, 2016.
- 1425 Wickham, H., François, R., Henry, L., Müller, K., and Vaughan, D.: dplyr: A Grammar of Data Manipulation, R package version
 1426 1.1.4, 2023a.
- 1427 Wickham, H., Pedersen, T. L., and Seidel, D.: scales: Scale Functions for Visualization, R package version 1.3.0, 2023b.
- 1428 Wietz, M., Engel, A., Ramondenc, S., Niwano, M., von Appen, W.-J., Priest, T., von Jackowski, A., Metfies, K., Bienhold, C., and
 1429 Boetius, A.: The Arctic summer microbiome across Fram Strait: Depth, longitude, and substrate concentrations structure
 1430 microbial diversity in the euphotic zone, *Environmental Microbiology*, 26, e16568, [https://doi.org/10.1111/1462-](https://doi.org/10.1111/1462-2920.16568)
 1431 2920.16568, 2024.
- 1432 Wietz, M., van Pinxteren, M., Freese, H. M., Spröer, C., and Zeppenfeld, S.: Seasonal connectivity of microbes and
 1433 carbohydrates between ocean, cryosphere and atmosphere in Kongsfjorden (Svalbard, Arctic Ocean), to be submitted as
 1434 preprint, 2025.
- 1435 Willis, M. D., Leaitch, W. R., and Abbatt, J. P. D.: Processes Controlling the Composition and Abundance of Arctic Aerosol,
 1436 *Reviews of Geophysics*, 56, 621–671, <https://doi.org/10.1029/2018RG000602>, 2018.
- 1437 Wong, J. P. S., Tsagkaraki, M., Tsiotra, I., Mihalopoulos, N., Violaki, K., Kanakidou, M., Sciare, J., Nenes, A., and Weber, R. J.:
 1438 Effects of Atmospheric Processing on the Oxidative Potential of Biomass Burning Organic Aerosols, *Environ. Sci. Technol.*, 53,
 1439 6747–6756, <https://doi.org/10.1021/acs.est.9b01034>, 2019.
- 1440 Wurl, O. and Holmes, M.: The gelatinous nature of the sea-surface microlayer, *Marine Chemistry*, 110, 89–97,
 1441 <https://doi.org/10.1016/j.marchem.2008.02.009>, 2008.



- 1442 Xu, W., Ovadnevaite, J., Fossum, K. N., Lin, C., Huang, R.-J., Ceburnis, D., and O'Dowd, C.: Sea spray as an obscured source for
1443 marine cloud nuclei, *Nat. Geosci.*, 15, 282–286, <https://doi.org/10.1038/s41561-022-00917-2>, 2022.
- 1444 Yang, C., Zhou, S., Zhang, C., Yu, M., Cao, F., and Zhang, Y.: Atmospheric Chemistry of Oxalate: Insight Into the Role of Relative
1445 Humidity and Aerosol Acidity From High-Resolution Observation, *Journal of Geophysical Research: Atmospheres*, 127,
1446 e2021JD035364, <https://doi.org/10.1029/2021JD035364>, 2022.
- 1447 Yttri, K. E., Bäcklund, A., Conen, F., Eckhardt, S., Evangeliou, N., Fiebig, M., Kasper-Giebl, A., Gold, A., Gundersen, H., Myhre,
1448 C. L., Platt, S. M., Simpson, D., Surratt, J. D., Szidat, S., Rauber, M., Tørseth, K., Ytre-Eide, M. A., Zhang, Z., and Aas, W.:
1449 Composition and sources of carbonaceous aerosol in the European Arctic at Zeppelin Observatory, Svalbard (2017 to 2020),
1450 *Atmospheric Chemistry and Physics*, 24, 2731–2758, <https://doi.org/10.5194/acp-24-2731-2024>, 2024.
- 1451 Yu, H., Kaufman, Y. J., Chin, M., Feingold, G., Remer, L. A., Anderson, T. L., Balkanski, Y., Bellouin, N., Boucher, O., Christopher,
1452 S., DeCola, P., Kahn, R., Koch, D., Loeb, N., Reddy, M. S., Schulz, M., Takemura, T., and Zhou, M.: A review of measurement-
1453 based assessments of the aerosol direct radiative effect and forcing, *Atmospheric Chemistry and Physics*, 6, 613–666,
1454 <https://doi.org/10.5194/acp-6-613-2006>, 2006.
- 1455 Zäncker, B., Cunliffe, M., and Engel, A.: Eukaryotic community composition in the sea surface microlayer across an east–west
1456 transect in the Mediterranean Sea, *Biogeosciences*, 18, 2107–2118, <https://doi.org/10.5194/bg-18-2107-2021>, 2021.
- 1457 Zeppenfeld, S. and Schmidt, L.: Dissolved and particulate carbohydrates and inorganic ions in the sea surface microlayer and
1458 bulk water of Kongsfjorden (Autumn 2021/Spring 2022), <https://doi.org/10.1594/PANGAEA.982606>, 2025.
- 1459 Zeppenfeld, S., van Pinxteren, M., Engel, A., and Herrmann, H.: A protocol for quantifying mono- and polysaccharides in
1460 seawater and related saline matrices by electro-dialysis (ED) – combined with HPAEC-PAD, *Ocean Science*, 16, 817–830,
1461 <https://doi.org/10.5194/os-16-817-2020>, 2020.
- 1462 Zeppenfeld, S., van Pinxteren, M., van Pinxteren, D., Wex, H., Berdalet, E., Vaqué, D., Dall'Osto, M., and Herrmann, H.: Aerosol
1463 Marine Primary Carbohydrates and Atmospheric Transformation in the Western Antarctic Peninsula, *ACS Earth Space Chem.*,
1464 5, 1032–1047, <https://doi.org/10.1021/acsearthspacechem.0c00351>, 2021.
- 1465 Zeppenfeld, S., van Pinxteren, M., Hartmann, M., Zeising, M., Bracher, A., and Herrmann, H.: Marine carbohydrates in Arctic
1466 aerosol particles and fog – diversity of oceanic sources and atmospheric transformations, *Atmospheric Chemistry and Physics*,
1467 23, 15561–15587, <https://doi.org/10.5194/acp-23-15561-2023>, 2023.
- 1468 Zeppenfeld, S., Schaefer, J., van Pinxteren, M., and Schmidt, L.: Marine combined carbohydrates and inorganic ions in
1469 atmospheric total suspended particles across altitudes in the lower troposphere of Ny-Ålesund, Svalbard,
1470 <https://doi.org/10.1594/PANGAEA.982703>, 2025.
- 1471 Zhou, S., Gonzalez, L., Leithead, A., Finewax, Z., Thalman, R., Vlasenko, A., Vagle, S., Miller, L. A., Li, S.-M., Burekul, S.,
1472 Furutani, H., Uematsu, M., Volkamer, R., and Abbatt, J.: Formation of gas-phase carbonyls from heterogeneous oxidation of
1473 polyunsaturated fatty acids at the air–water interface and of the sea surface microlayer, *Atmospheric Chemistry and Physics*,
1474 14, 1371–1384, <https://doi.org/10.5194/acp-14-1371-2014>, 2014.
- 1475 Zhu, B., Sun-Waterhouse, D., and You, L.: Insights into the mechanisms underlying the degradation of xylooligosaccharides in
1476 UV/H₂O₂ system, *Carbohydrate Polymers*, 317, 121091, <https://doi.org/10.1016/j.carbpol.2023.121091>, 2023.
- 1477 Zhu, Y.-S., Connolly, A., Guyon, A., and FitzGerald, R. J.: Solubilisation of calcium and magnesium from the marine red algae
1478 *Lithothamnion calcareum*, *International Journal of Food Science and Technology*, 49, 1600–1606,
1479 <https://doi.org/10.1111/ijfs.12459>, 2014.